Shuttling Rates, Electronic States, and Hysteresis in a Ring-in-Ring Rotaxane

Mark C. Lipke,[1] Yilei Wu,[2] Indranil Roy,[2] Yuping Wang,[2] Michael R. Wasielewski,[2] J. Fraser Stoddart[2*]

[1] *Department of Chemistry and Chemical Biology, Rutgers The State University of New Jersey, 610 Taylor Road, Piscataway NJ 08854*
[2]*Department of Chemistry, Northwestern University, 2145 Sheridan Road, Evanston, IL 60208 (USA)*

Supporting Information

Table of Contents

1. General Considerations

Commercially available chemicals were purchased and used as received without further purification - (1) from Aldrich: dimethyl-5-aminoisophthalate, propargyl bromide, $LiAlH_4$, $NaNO_2$, and PBr_3, and (2) from Alfa-Aesar: 4,4'-bipyridine and NaN_3. The compounds cyclobis(paraquat-*p*-biphenylene) tetrakis(hexafluorophosphate)[1] (**MS**•$4PF_6$), 1-(prop-3-ynoxy)-4-(tris-(4-tert-butyl-phenyl)-methyl)-benzene,[2] and 3,5-bis(hydroxymethyl)aniline[3] were prepared as reported previously in the literature. For all reactions and measurements using MeCN, the solvent was deoxygenated by sparging with Ar and dried using solvent purification columns supplied by Pure Process Technologies. Deuterated solvents (CD_3CN, $CDCl_3$, CD_3SOCD_3, and CD_3COCD_3) were purchased from Cambridge Isotopes and used as received unless otherwise stated. All UV-Vis-NIR spectra were recorded using a Shimadzu UV-3600 spectrophotometer equipped with a temperature controlled cuvette holder. Routine characterization by nuclear magnetic resonance spectroscopy (NMR) was performed using a Bruker Avance III spectrometer with a 500 MHz working frequency for ^1H nuclei and 125 MHz for ^{13}C nuclei. Variable temperature ^1H NMR spectra were recorded using an Agilent DD2 spectrometer with a 500 MHz working frequency for ^1H nuclei. Diffusion ordered NMR spectra (DOSY) were recorded using an Agilent DD2 spectrometer with a 600 MHz working frequency for ^1H nuclei. All NMR spectra were referenced to the residual proteo solvent signal (CD_3CN: ^1H 1.94 ppm; $CDCl_3$: ^1H 7.24 ppm, CD_3SOCD_3: 2.50 ppm, and CD_3COCD_3: 2.05 ppm). High resolution mass spectra were measured using a Thermo Finnegan LCQ ion-trap mass spectrometer with electrospray ionization. Cyclic voltammograms were recorded using a Gamry Reference 600 potentiostat with a glassy carbon working electrode, platinum wire counter electrode, and a silver wire pseudo-reference electrode on sample under and argon atmosphere with ferrocene added as an internal redox standard. Samples for cyclic voltammetry were prepared using an electrolyte solution of 0.1 M $[Bu_4N][PF_6]$ in MeCN that was sparged with Ar to remove O_2. Digital simulations of the CV data were performed using DigiSim. Elaborations on the above experimental details are provided below in the appropriate sections.

2. Synthetic Details

The **BoxInBoxRotaxane**•8PF_6 (**BBR**•8PF_6) was prepared by the route depicted in Scheme S1. Synthetic procedures and characterization data are reported on subsequent pages for **BBR**•8PF_6 and all other new compounds. The starting material 3,5-bis(hydroxymethyl)aniline (**1**) was prepared from the commercially available compound, dimethyl-5-aminoisophthalate, following a literature procedure.[3]

Scheme S1. Synthesis of BBR•8PF_6.

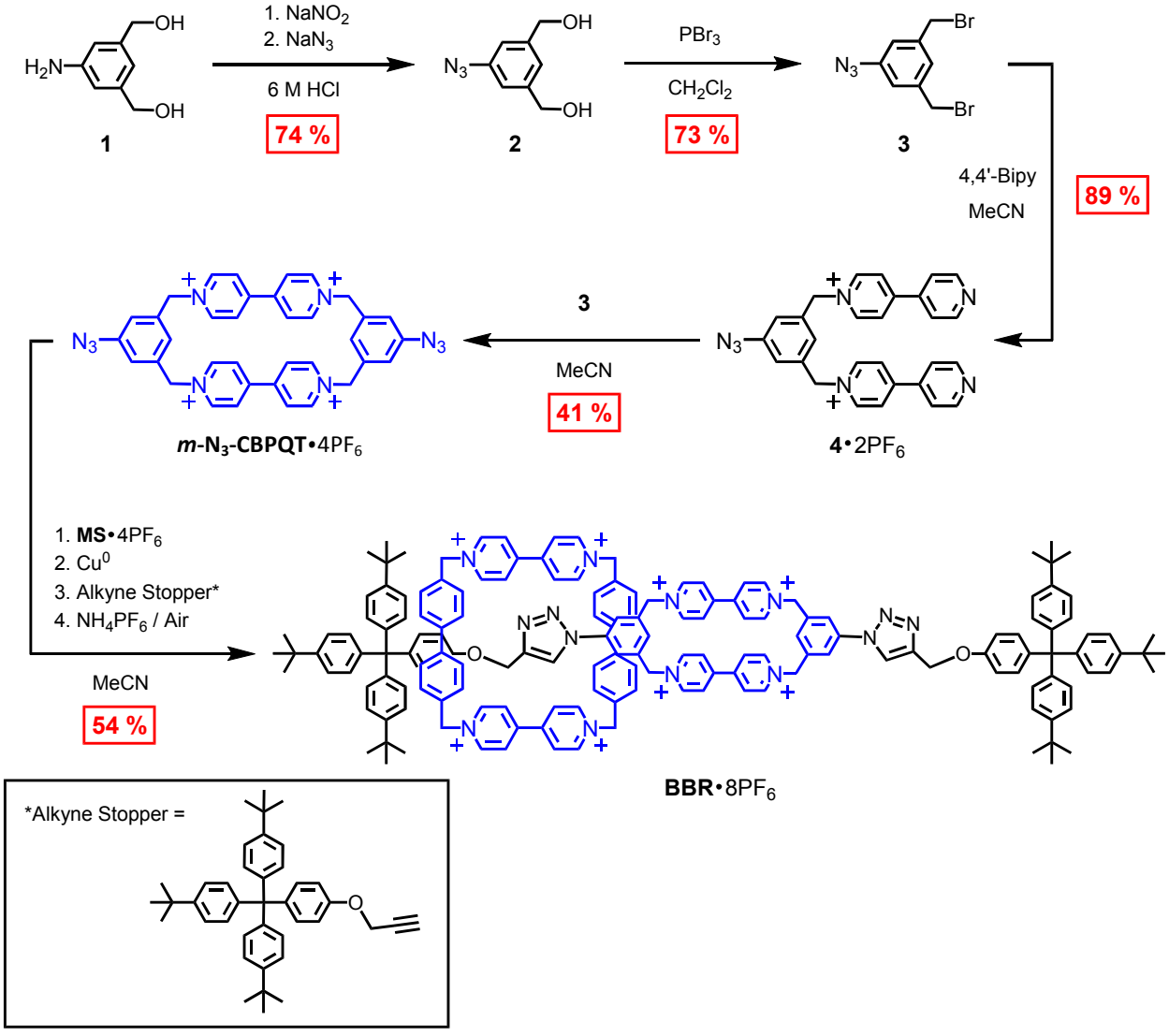

α,α'-Dihydroxy-3-azido-*m*-xylene (2)

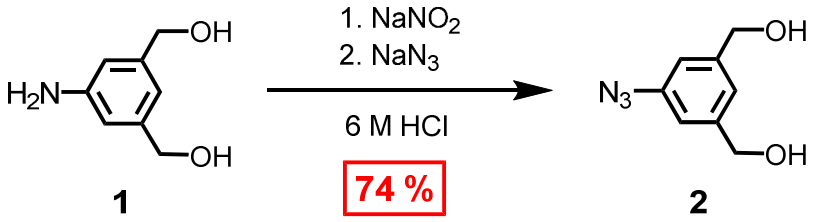

3,5-Bis(hydroxymethyl)aniline (**1**, 3.13 g, 20.4 mmol) was dissolved in of 6 M aqueous hydrochloric acid (30 mL) to give a yellow solution. This solution was cooled in an ice bath for 30 min prior to starting the dropwise addition of an ice-cold aqueous solution $NaNO_2$ (2.0 g, 29.0 mmol, 15 mL water). The reaction mixture was kept in the ice bath and stirred vigorously during the addition of the $NaNO_2$ solution over 20 min. After stirring for an additional 30 min, an ice-cold aqueous solution of NaN_3 (5.25 g, 80.8 mmol, 50 mL water) was added to the reaction solution over 30 min. Addition of the NaN_3 solution was initially conducted in a dropwise manner, and was accompanied by considerable gas evolution that eventually subsided enough to permit addition of the NaN_3 solution in portions. A pale tan precipitate began forming after approximately half of the NaN_3 had been added. Stirring was continued for 12 h while the reaction mixture and ice bath were allowed to warm to room temperature. The precipitate was collected by filtration, washed several times with H_2O, and then air dried to provide the pure product **2** as a pale tan powder (2.73 g, 74 % yield). ^{1}H NMR (500 MHz, $CDCl_3$): δ 7.12 (1H), 6.96 (2H), 4.69 (d, J = 5.7 Hz, 4H), 1.69 (t, J = 5.7 Hz, 2H). $^{13}C\{^1H\}$ (125 MHz, $CDCl_3$) δ 143.4, 140.9, 121.7, 116.7, 64.9. HRMS (ESI): m/z Calcd for $C_8H_8N_3O_2$: 178.0622, found: 178.0617 $[M - H]^-$.

α,α'-Dibromo-3-azido-*m*-xylene (3)

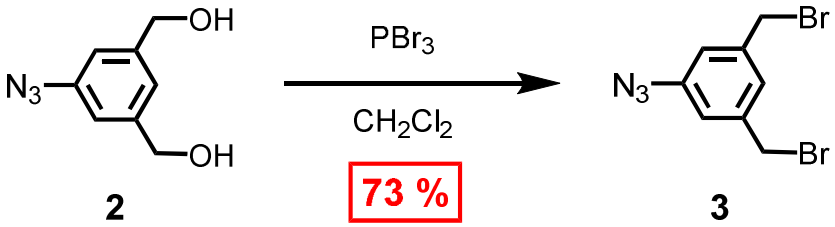

α,α'-Dihydroxy-3-azido-*m*-xylene (**2**, 1.70 g, 9.49 mmol) was dissolved in dry CH_2Cl_2 (80 mL) under and atmosphere of N_2. This solution was stirred and cooled in an ice bath for 30 min prior to the addition of neat PBr_3 (2.50 mL, 26.4 mmol) over 10 min *via* syringe. The reaction mixture was removed from the ice bath and the reaction progress was monitored by recording ^1H NMR spectra of aliquots that were removed and processed as described below for the initial work-up of the full reaction mixture. After 20 h, an additional 0.5 mL of PBr_3 (5.28 mmol) was added and the reaction mixture was stirred for 5 h prior to being poured into ice and water (150 mL). The organic layer was separated and the aqueous solution was extracted with CH_2Cl_2 (150 mL). The combined organic layers were washed with H_2O (2 x 100 mL) before drying over $MgSO_4$ and evaporating under reduced pressure (note that aliquots were similarly processed while monitoring the reaction). This procedure provided a yellow oil that crystallized while standing overnight. The crude product was extracted with hexanes (2 x 250 mL), and the resulting solutions were combined and evaporated to provide the pure product **3** as white crystals (2.09 g, 73 % yield). ^1H NMR (500 MHz, $CDCl_3$): δ 7.16 (t, J = 1.3 Hz, 1H), 6.96 (d, J = 1.3 Hz, 2H), 4.41 (4H). $^{13}C\{^1H\}$ (125 MHz, $CDCl_3$) δ 141.3, 140.4, 126.2, 119.7, 32.1. HRMS analysis failed to confirm the identity of the product **3**, but the NMR characterization and subsequent use of the product in the synthesis of **4**•2PF_6 and **5**•4PF_6 demonstrate that the desired dibromo compound **3** was obtained.

[α,α'-Bis(4-pyridylpyridinium)-3-azido-*m*-xylene]•2PF_6 (4•2PF_6)

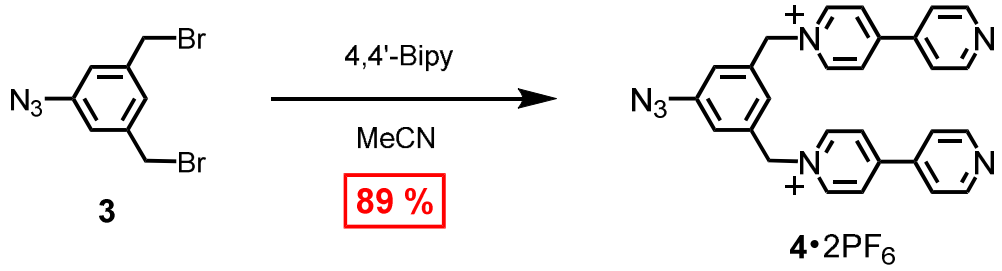

A syringe pump was used to add, over the course of 1 h, a solution of α,α'-dibromo-3-azido-*m*-xylene (**3**, 0.597 g, 1.96 mmol) in dry MeCN (20 mL) to a stirred solution of 4,4'-bipyridine

(3.50 g, 22.4 mmol) in dry MeCN (75 mL) under reflux in an N_2 atmosphere. Stirring and heating were continued for an additional 2 h, during which a pale green precipitate formed. After allowing the reaction mixture to cool to room temperature, the precipitate was collected by filtration and washed with MeCN (2 x 25 mL) and then CH_2Cl_2 (3 x 50 mL). The crude product was dissolved in MeOH (200 mL) to provide a clear yellow solution that was added to a solution of NH_4PF_6 (5 g) in H_2O (100 mL). This procedure resulted in the formation of voluminous white crystals that were collected by filtration, washed with H_2O (3 x 50 mL), and dried under air to provide the pure product **4**•2PF_6 as an off-white powder (1.297 g, 89 % yield). ^{1}H NMR (500 MHz, CD_3CN): δ 8.81 – 8.86 (overlapping multiplets, 8H), 8.33 (d, J = 7.1 Hz, 4H), 7.78 (m, 4H), 7.31 (t, J = 1.2 Hz, 1H), 7.28 (d, J = 1.2 Hz, 2H), 5.73 (4 H). ^{13}C{^{1}H} (125 MHz, CD_3CN) δ 156.2, 152.6, 146.5, 144.0, 142.4, 137.2, 127.6, 127.6, 123.2, 122.5, 64.4. HRMS (ESI): *m*/*z* Calcd for $C_{28}H_{23}N_7F_6P$: 602.1651, found: 602.1656 [M – PF_6]$^+$.

Bis-azide-*m*-CBPQT•4PF_6 (*m*-N_3-CBPQT•4PF_6)

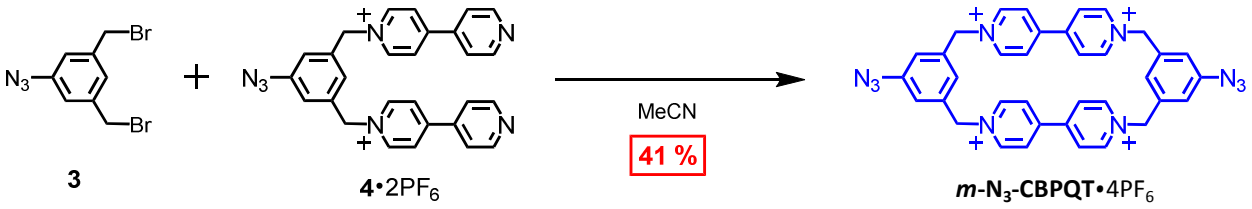

A double syringe pump was used to add simultatneously, over the course of 50 h, a solution of [α,α'-bis(4-pyridylpyridinium)-3-azido-*m*-xylene]•2PF_6 (**4**•2PF_6, 0.637 g, 0.852 mmol) in MeCN (50 mL) and a solution of α,α'-dibromo-3-azido-*m*-xylene (**3**, 0.275 g, 0.902 mmol) in MeCN (50 mL) to dry MeCN (150 mL) under reflux with stirring in an N_2 atmosphere. Heating and stirring was continued for 3 days, after which the mixture had turned yellow and an off-white precipitate had formed. The reaction mixture was allowed to cool to room temperature and the precipitate was collected by filtration. The insoluble crude product was suspended in MeCN (20 mL) and treated with conc. aqueous HCl (2 mL). After stirring for 10 min, the solids were

collected by filtration, dissolved in H_2O (10 mL), and added to an aqueous solution of NH_4PF_6. The resulting white precipitate was collected by filtration, washed with H_2O (3 x 5 mL), and dried under air to provide an off-white powder. This powder was dissolved in MeCN (10 mL), the solution was filtered to remove a small amount of insoluble material, and the solvent was evaporated under reduced pressure to provide a white powder. The product was washed sparingly with Me_2CO (3 x 2 mL) and dried under air to provide pure **5**•4PF_6 as a white powder (0.413 g, 41 % yield). ^{1}H NMR (500 MHz, CD_3CN): δ 8.75 (d, J = 6.7 Hz, 8H), 8.08 (d, J = 6.7 Hz, 8H), 7.48 (d, J = 1.2 Hz, 4H), 6.72 (t, J = 1.2 Hz, 2H), 5.76 (8H). $^{13}C\{^1H\}$ (125 MHz, CD_3CN) δ 151.4, 147.0, 143.9, 138.0, 128.6, 124.8, 123.3, 65.1. HRMS (ESI): *m*/*z* Calcd for $C_{36}H_{30}N_{10}F_{18}P_3$: 1037.1575, found: 1037.570 $[M - PF_6]^+$.

BoxInBoxRotaxane•8PF_6 (BBR•8PF_6)

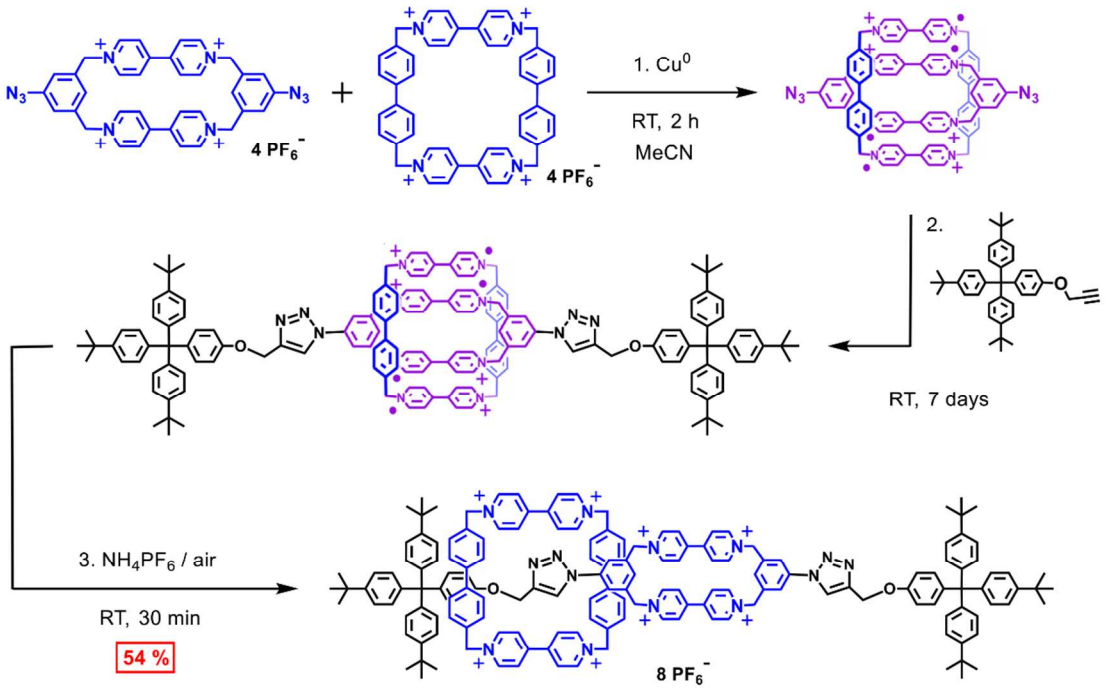

Bis-azide-*m*-CBPQT•4PF_6 (**5**•4PF_6, 37.7 mg, 0.0319 mmol) and **MS**•4PF_6 (43.5 mg, 0.0347 mmol) were dissolved in dry MeCN (25 mL) under the N_2 atmosphere of a glovebox to give a clear, pale yellow solution. This solution was stirred over an excess of Cu^0 powder (~1 g) for 3 h

to provide a dark purple solution. The stoppering reagent 1-(prop-3-ynoxy)-4-(tris-(4-tert-butyl-phenyl)-methyl)-benzene (43.5 mg, 0.0802 mmol) was added as a powder and stirring was continued for 7 days. An excess of NH_4PF_6 (~200 mg) was added and the mixture was removed from the glovebox and stirred under air until the purple color had faded entirely. The resulting cloudy yellow solution was filtered and solvent was evaporated under reduced pressure to provide a yellow solid. The crude product was washed with H_2O (3 x 3 mL) and CH_2Cl_2 (3 x 2 mL) to remove excess NH_4PF_6 and excess stoppering reagent, respectively. The crude product was dissolved in MeCN (5 mL) and treated with a solution of Bu_4NCl (~100 mg) in MeCN (2 mL) to precipitate the product as its chloride salt. The precipitate was collected by filtration and washed with MeCN (2 x 3 mL) and then H_2O (4 x 3 mL) to remove excess **MS**•4Cl. The remaining solids were dissolved in MeOH (5 mL) and added to a solution of NH_4PF_6 (100 mg) in H_2O (5 mL) to precipitate the partially purified product. The suspension was concentrated under reduced pressure and the solids were collected by filtration, washed with H_2O (3 x 3 mL), and air dried. The product was dissolved in MeCN (10 mL) under the N_2 atmosphere of a glovebox and reduced by stirring over excess zinc dust for 45 min. The resulting dark purple solution was filtered and the product was precipitated by vapor diffusion with $^{i}Pr_2O$. The resulting dark purple, microcrystalline powder was collected by filtration and washed with the remaining anti-solvent. The dark purple product was dissolved in MeCN (15 mL), NH_4PF_6 (~200 mg) was added, and the solution was stirred under air until the purple color had entirely faded. The resulting yellow solution was filtered and solvent was evaporated under reduced pressure to provide a yellow powder that was washed with water (3 x 5 mL) and air dried. This provided pure **BBR**•8PF_6 as a pure yellow powder (61 mg, 54 % yield). ^{1}H NMR (500 MHz, CD_3CN): δ 8.88 (d, *J* = 6.9 Hz, 8H), 8.85 (d, *J* = 6.6 Hz, 4H), 8.84 (d, *J* = 6.6 Hz, 4H), 8.54 (1H), 8.29 (2H), 8.18 (2H), 8.17 (d, *J* = 6.6 Hz, 4H), 8.16 (d, *J* = 6.6 Hz, 4H), 8.05 (1H), 7.86 (d, *J* = 6.9 Hz, 8H), 7.53 (16 H), 7.48 (d, *J* = 8.7 Hz, 6H), 7.31 – 7.35 (overlapping doublets, *J* = 8.7 Hz each, 6H each), 7.21 (d, *J* = 8.7 Hz, 2H), 7.19 (d, *J* = 8.7, 6H), 7.07 (1H), 7.05 (1H), 7.00 (d, *J* = 8.7 Hz, 2H), 6.72 (d, *J* = 8.7 Hz, 2H), 5.98 (4H), 5.91 (4H), 5.79 (8H), 5.29 (2H), 4.57 (d, *J* = 8.7 Hz, 2H), 3.17 (2 H), 1.33 (27H), 1.29 (27H). $^{13}C\{^1H\}$ (125 MHz, CD_3CN) δ 156.8, 155.0, 150.8 (2 overlapping signals), 149.6, 149.1, 146.5, 146.4, 145.8, 145.6, 145.1, 143.2, 141.7, 141.1, 140.9, 138.7, 138.5, 137.2 (2 overlapping signals), 137.2, 134.7, 132.4, 131.8, 130.8, 130.5, 130.3, 130.2, 128.4, 128.4, 128.1, 128.0, 127.9, 127.8, 125.6, 125.1, 123.9, 123.8, 122.9, 122.8, 114.2, 112.5, 65.4, 64.3, 64.2, 63.8, 63.7, 61.9, 60.3, 34.7, 34.6, 31.2, 31.2. HRMS (ESI):

m/*z* Calcd for $C_{164}H_{162}N_{14}F_{36}P_6$: 1615.0439, found: 1615.0422 $[M - 2PF_6]^{2+}$; and *m*/*z* Calcd for $C_{164}H_{162}N_{14}F_{30}P_5$: 1028.3743, found: 1028.3741 $[M - 3PF_6]^{3+}$

m-Box-Dumbbell•4PF_6 (*m*-BDB•4PF_6)

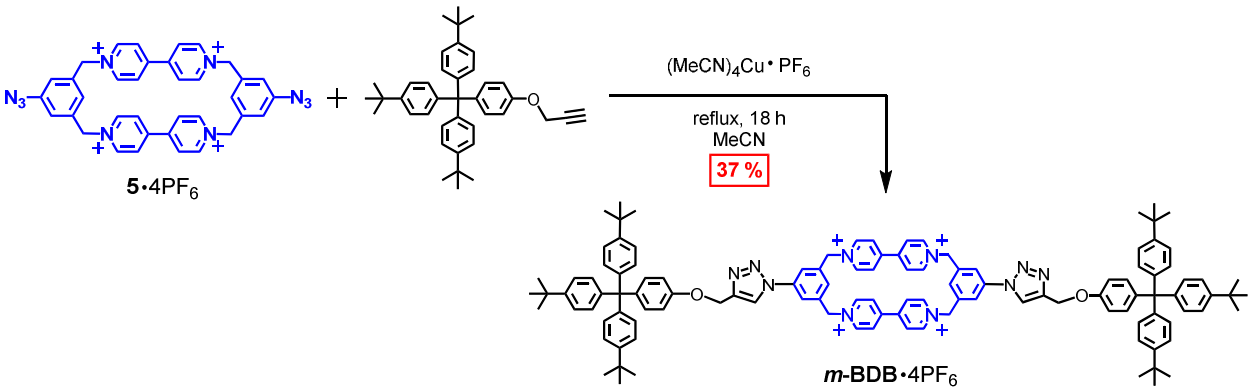

1-(prop-3-ynoxy)-4-(tris-(4′-tertbutylphenyl)-methyl)-benzene (28 mg, 0.054 mmol), bis-azide-*m*-CBPQT•4PF_6 (**5**•4PF_6, 20 mg, 0.017 mmol), and tetrakis(acetonitrile)copper(I)-hexafluorophosphate (8 mg, 0.02 mmol) were dissolved in dry, deoxygenated tetrahydrofuran (10 mL) under an N_2 atmosphere in a round-bottom flask fitted with a reflux condenser. The resulting solution was stirred and heated under reflux for 18 h. The reaction mixture was then allowed to cool before solvent was removed under vacuum. The resulting residue was washed with diethyl ether (3 x 20 mL) and ethyl acetate (3 x 20 mL) to provide a yellow powder that was dissolved in acetonitrile and centrifuged to remove a small amount of fine, insoluble impurities. Further purification was achieved *via* preparative reverse-phase HPLC, eluting with a mixture of MeCN and 1% trifluoroacetic acid in H_2O. MeCN was evaporated from the resulting eluent under vacuum, and pure ***m*-BDB**•4PF_6 (21 mg, 37 %) was precipitated as a pale yellow powder by the addition of excess aqueous NH_4PF_6. ^{1}H NMR (500 MHz, CD_3CN): δ 8.84 (d, J = 6.8 Hz, 8H), 8.55 (s, 2H), 8.31 (s, 4H), 8.13 (d, J = 6.9 Hz, 8H), 7.37 (d, J = 6.8 Hz, 12 H), 7.25 (d, J = 6.55 Hz, 12 H), 7.22 (d, J = 8.9 Hz, 4 H), 7.07 (s, 2 H), 7.03 (d, J = 8.9 Hz, 4H), 5.92 (s, 8H), 5.32 (s, 4H), 1.32 (s, 54 H). ^{13}C NMR (125 MHz, CD_3CN): δ 150.7, 149.7, 149.2, 146.4, 146.9, 145.1, 141.0, 137.2, 132.4, 131.8, 130.8, 127.9, 125.1, 123.9, 118.8, 122.9, 114.2, 65.3, 64.6, 62.9, 35.6, 32.1. HRMS (ESI) For ***m*-BDB**•4PF_6, Calcd for $C_{116}H_{122}F_{24}N_{10}O_2P_4$: 988.9535 $[M\text{-}2PF_6]^{2+}$; found: 988.9526 $[M\text{-}2PF_6]^{2+}$.

3. Routine 1D and 2D NMR Characterization

Nuclear magnetic resonance spectroscopy (NMR) was performed using a Bruker Avance III spectrometer with a 500 MHz working frequency for ^{1}H nuclei and 125 MHz for ^{13}C nuclei. Diffusion-ordered NMR spectra were recorded using an Agilent DD2 spectrometer with a 600 MHz working frequency for ^{1}H nuclei. All NMR spectra were referenced to the residual proteo solvent signal (CD_3CN: ^{1}H 1.94 ppm). A small number of resonances could not be assigned definitively to a single proton position out of multiple positions in **BBR**$^{8+}$, **BBR**$^{4(+\bullet)}$, ***m*-DBD**$^{4+}$, and ***m*-DBD**$^{2(+\bullet)}$ that give rise to peaks with similar chemical shifts and coupling patterns. These resonances and protons are assigned duplicate labels.

BBR•8PF$_6$ and BBR$^{4(+\bullet)}$

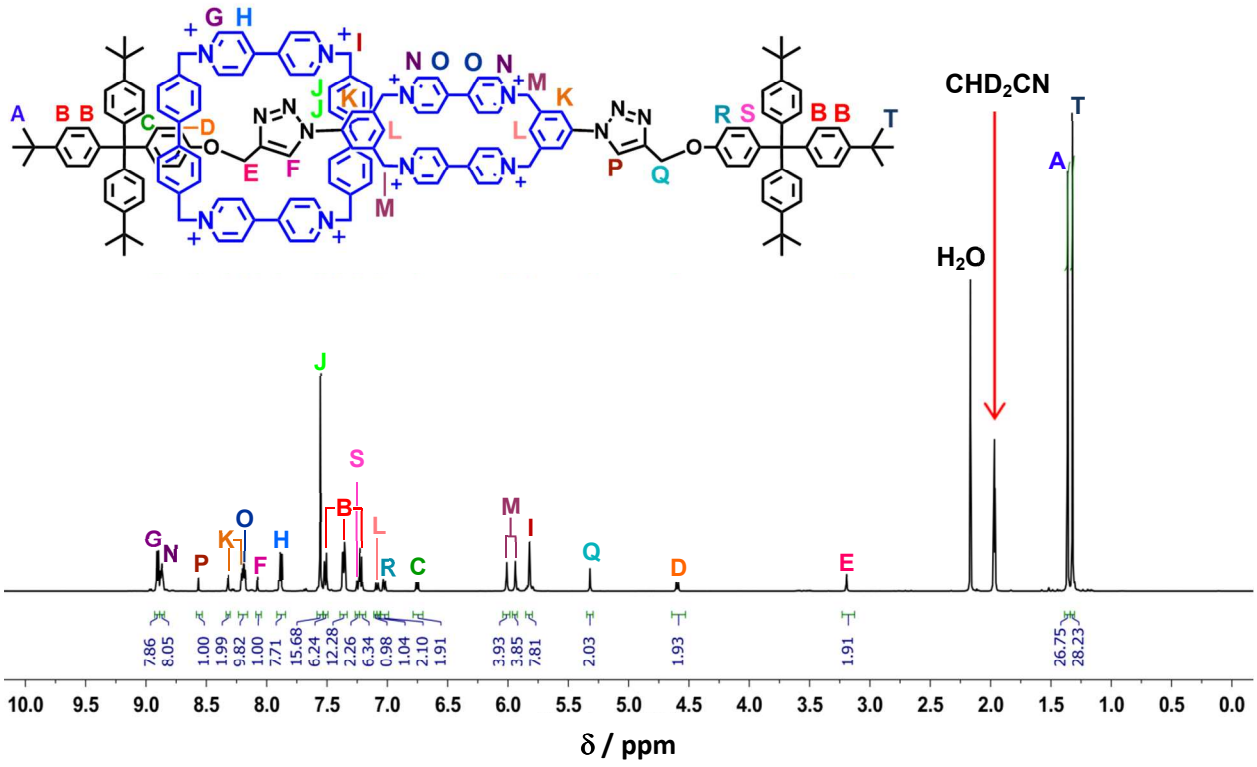

Figure S1. ^{1}H NMR spectrum of **BBR**•8PF$_6$ in CD_3CN.

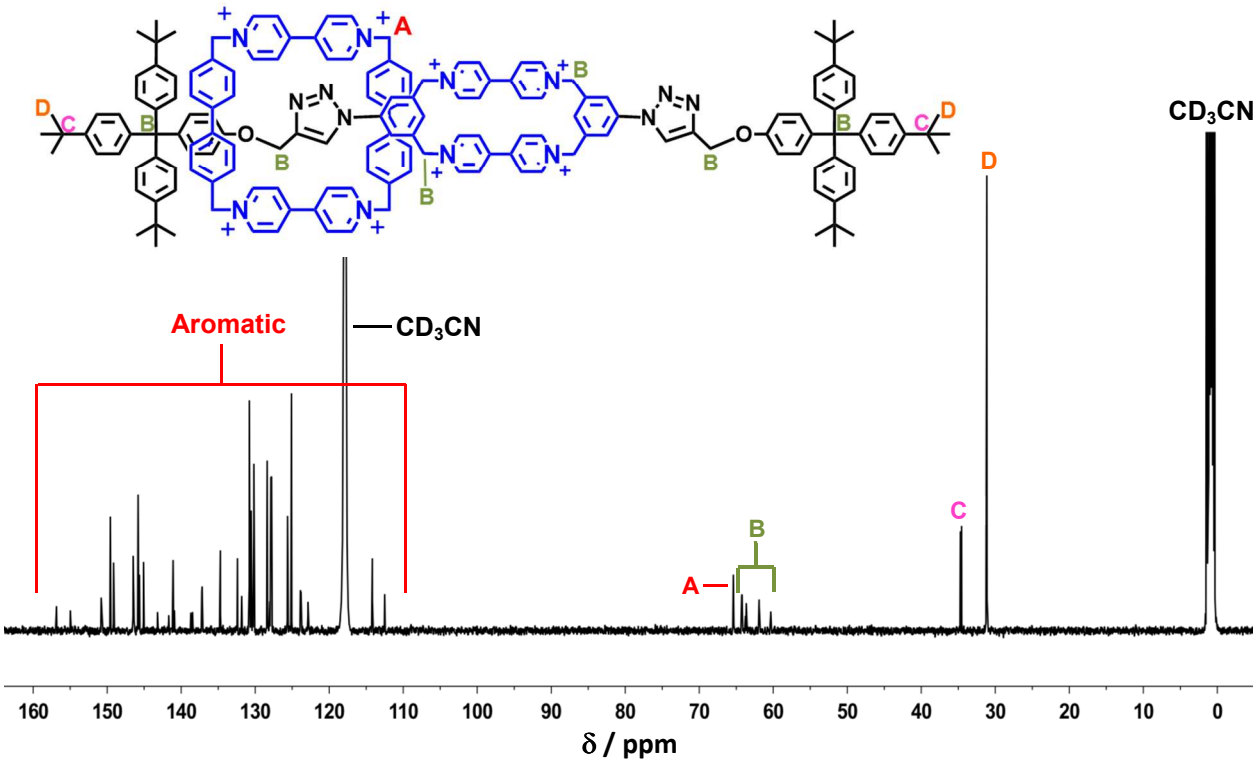

Figure S2. $^{13}C\{^{1}H\}$ NMR spectrum of **BBR**•8PF_6 in CD_3CN.

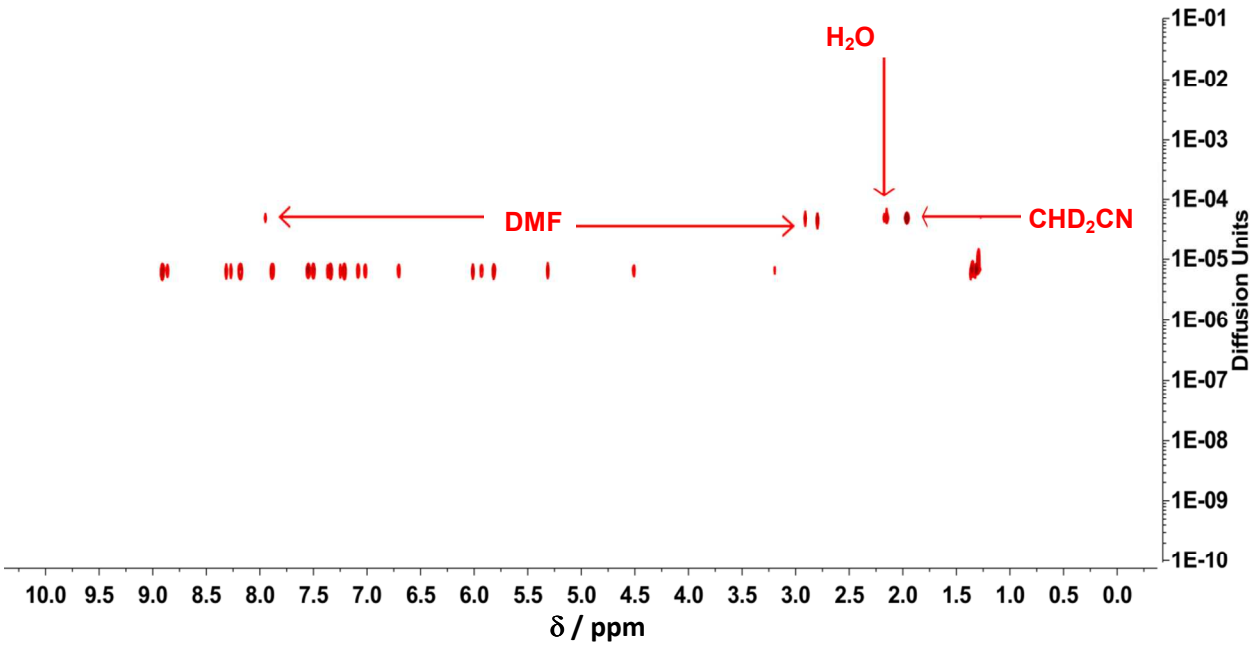

Figure S3. Diffusion ordered (DOSY) ^{1}H NMR spectrum of **BBR**•8PF_6 in CD_3CN. All unlabeled signals correspond to $\mathbf{BBR}^{8+}$. Note that this NMR sample contained a small amount of DMF that was inadvertently introduced via a contaminated pipette bulb while preparing the sample, but this mishap does not affect the DOSY measurement.

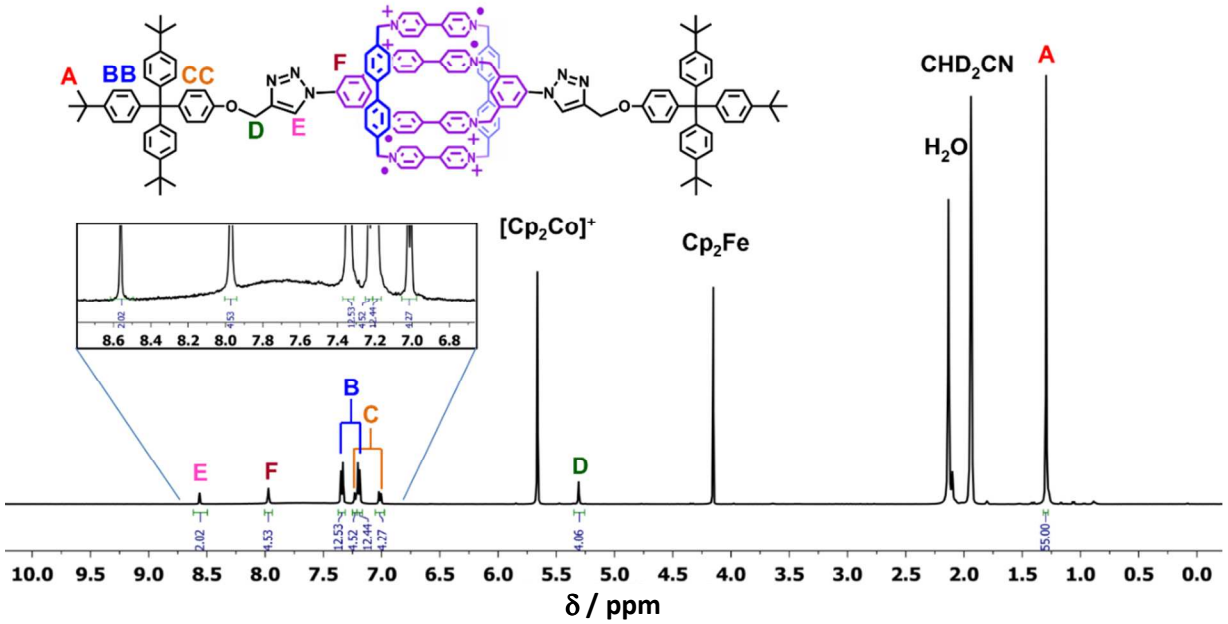

Figure S4. ^{1}H NMR spectrum of **BBR**•8PF_6 in CD_3CN with 4 equiv of Cp_2Co added to form **BBR**$^{4(+\bullet)}$. The inset displays a broad resonance observed in the aromatic region. A sealed capillary containing a solution of Cp_2Fe in CD_3CN was included as an internal standard.

m-BDB•4PF_6 and *m*-BDB$^{2(+\bullet)}$

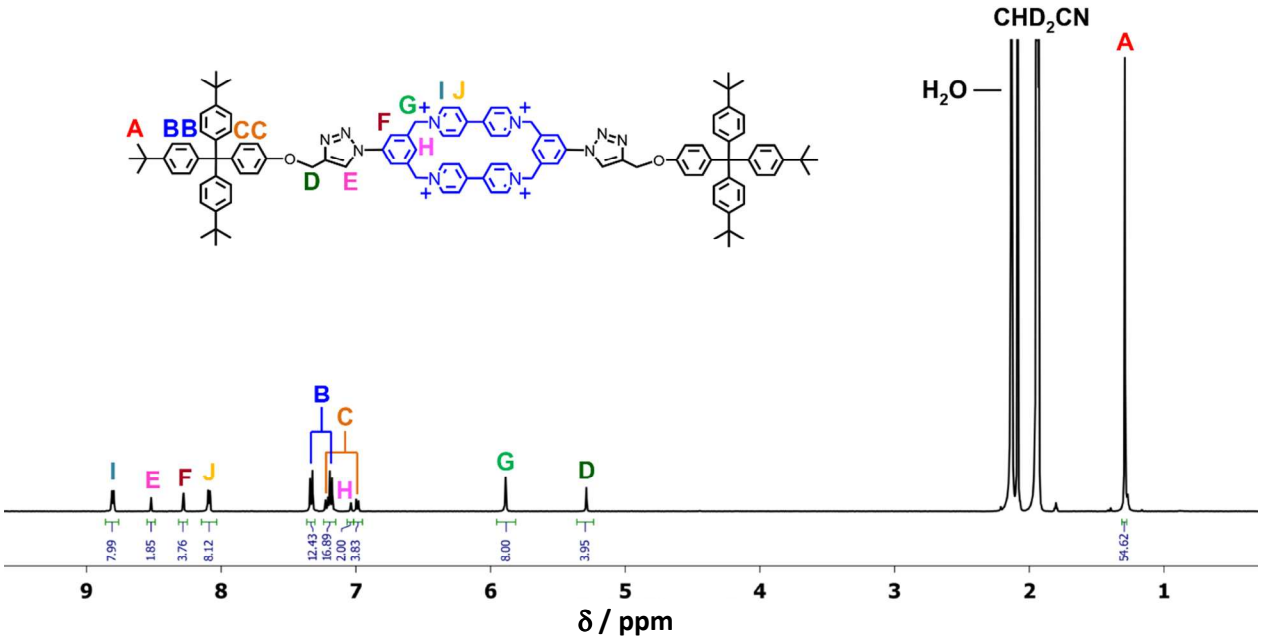

Figure S5. ^{1}H NMR spectrum of ***m*-BDB**•4PF_6 in CD_3CN.

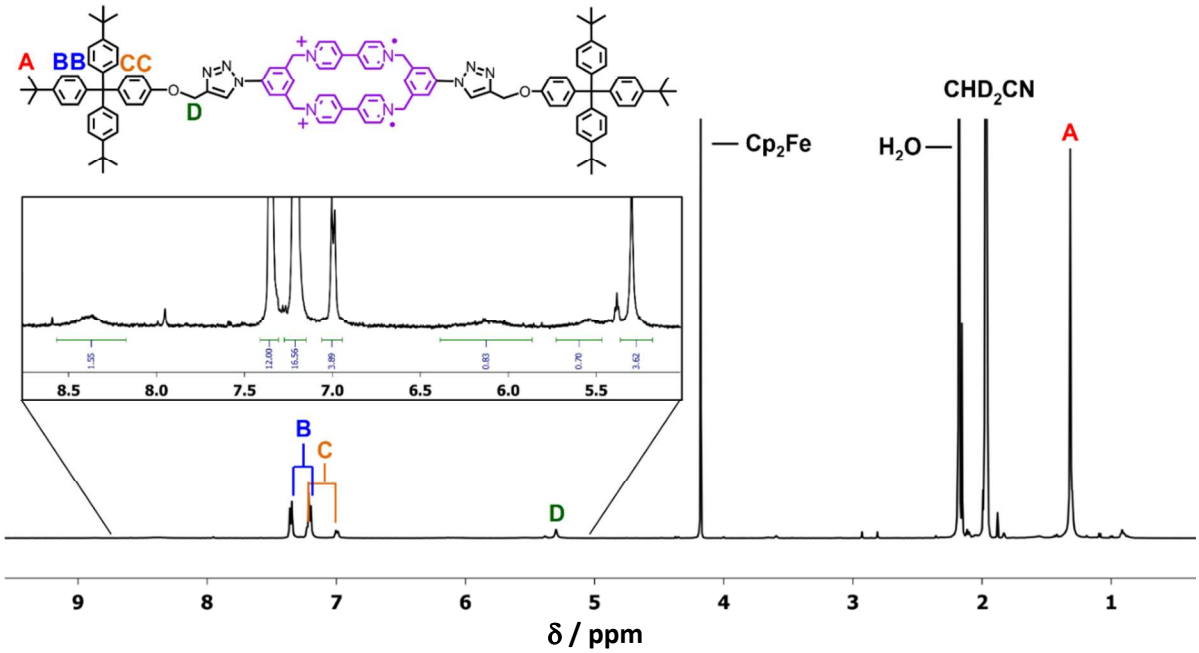

Figure S6. ^{1}H NMR spectrum of a solution of ***m*-BDB$^{2(+\bullet)}$** in CD_3CN that was prepared by stirring a solution of ***m*-BDB•4PF$_6$** in CD_3CN over Zn dust for 15 min. A sealed capillary containing a solution of Cp_2Fe in CD_3CN was included as an internal standard.

^{1}H NMR Spectrum of *o*-CBPQT•4PF$_6$

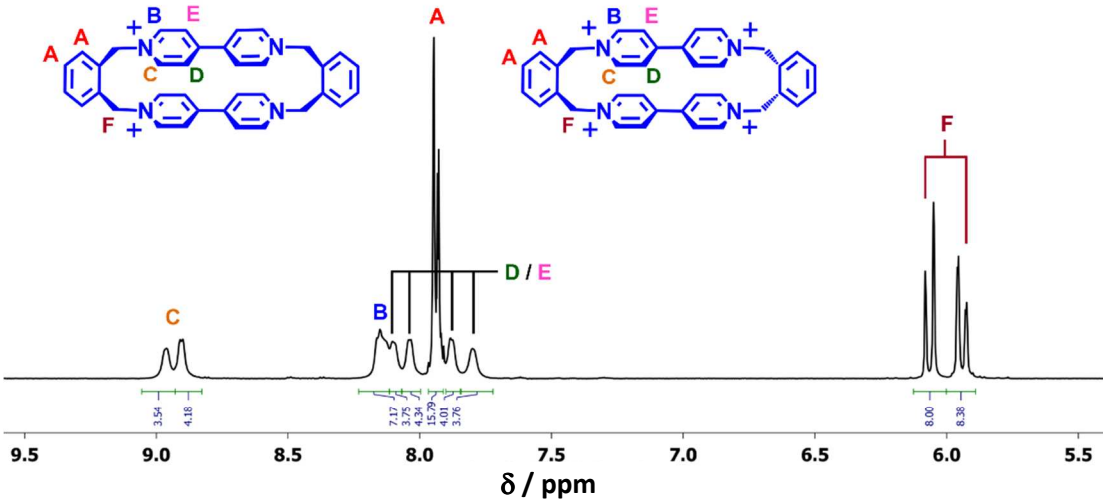

Figure S7. ^{1}H NMR spectrum of ***o*-CBPQT•PF$_6$** in CD_3CN. Two distinct conformers of the cyclophane are present, giving rise to two sets of similar NMR resonances for all of the aromatic proton positions. The methylene groups are also observed as two distinct resonances (two doublets, J = 16 Hz), which in this case is due to diastereotopic protons that exhibit overlapping resonances for the two conformers.

^{1}H NMR Spectrum of *o*-CBPQT$^{2(+\bullet)}$

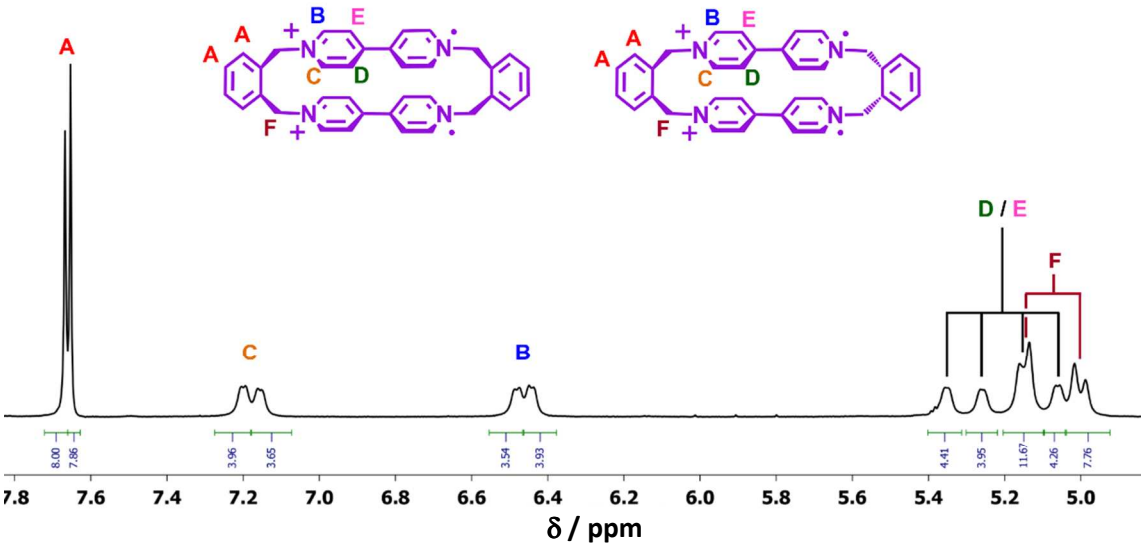

Figure S8. ^{1}H NMR spectrum of a 1 mM solution of ***o*-CBPQT$^{2(+\bullet)}$** (prepared by stirring a solution of ***o*-CBPQT**•4PF_6 over Zn) in CD_3CN. As with the tetracationic form of this cyclophane, two distinct conformers of the cyclophane are present, giving rise to two sets of similar NMR resonances for all of the aromatic proton positions. The methylene groups are also observed as two distinct resonances (two doublets, J = 14 Hz), which is due to diastereotopic protons that exhibit overlapping resonances for the two conformers.

4. Routine UV-Vis-NIR Characterization

Stock solutions of the octacationic **BBR^{8+}** were prepared by dissolving suitable amounts of the **BBR**•8PF_6 in air-free MeCN to provide 0.5 or 1 mM concentrations. Syringes were used to dilute these stock solutions to the desired concentrations for measurement prior to stirring over activated Zn dust for 15 min to form dark magenta-purple solutions of the tetraradical tetracation **BBR$^{4(+\bullet)}$**. These solutions were filtered and transferred to a 1.0 cm quartz cuvette for recording spectra. Alternatively, solutions of **BBR**•8PF_6 were reduced inside the cuvette by the addition of 4 equiv of Cp_2Co in MeCN. The concentration of the Cp_2Co stock solution was calibrated prior to use by the addition of a known volume to an excess of **MV**•2PF_6 solution, followed by measuring the resulting concentration of **MV$^{(+\bullet)}$** by UV-Vis-NIR spectroscopy.

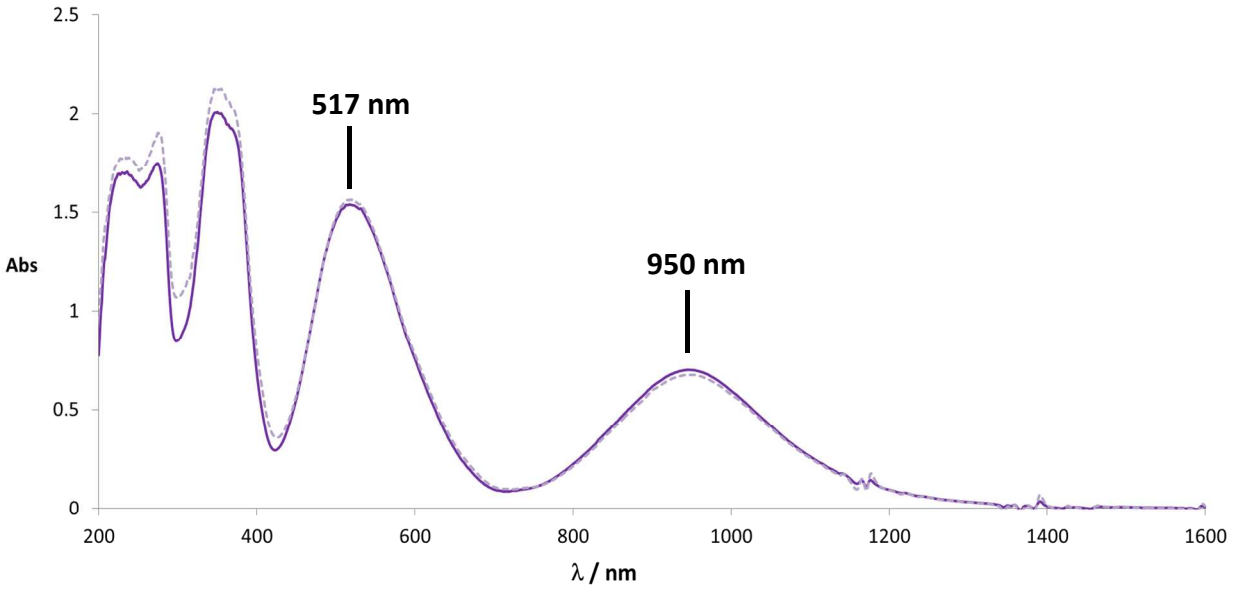

Figure S9. UV-Vis-NIR spectra of 0.050 mM $\mathbf{BBR}^{4(+\bullet)}$ recorded at 298 K in a 1.0 cm path cell. The solid purple trace is from a sample prepared by reduction of $\mathbf{BBR}^{8+}$ over Zn dust, and the faded dashed trace results from a sample prepared by addition of 4 equiv of Cp_2Co to a solution of $\mathbf{BBR}^{8+}$. The NIR-absorption (λ_{max} = 950 nm) is very similar to that[4] of the supramolecular complex $\mathbf{[MS\square m\text{-}CBPQT]}^{4(+\bullet)}$ (λ_{max} = 941 nm).

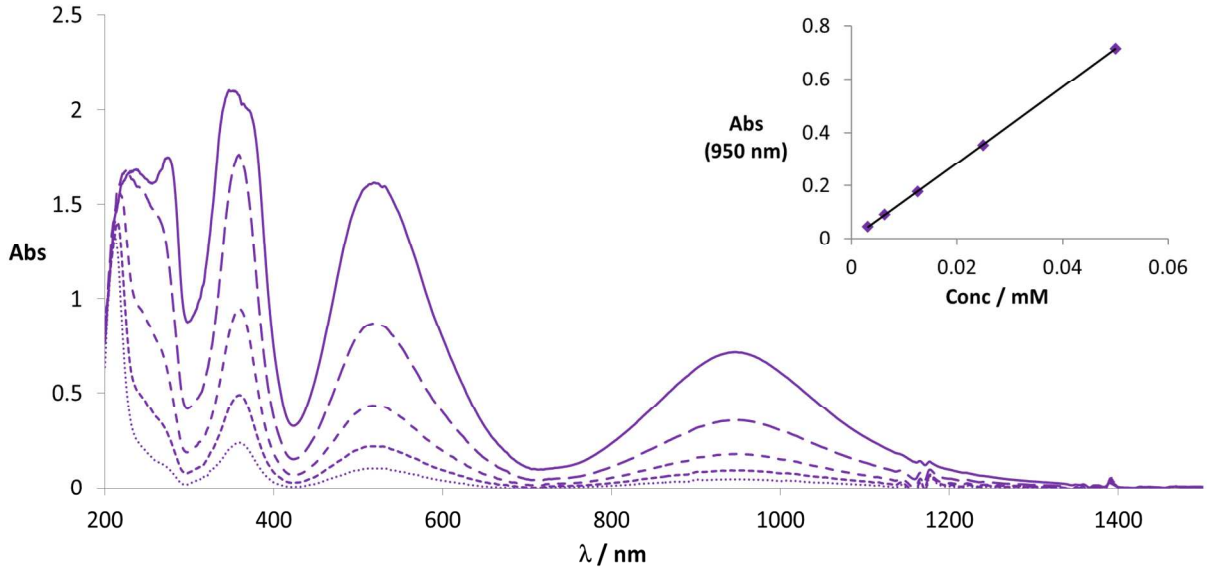

Figure S10. UV-Vis-NIR spectrum of $\mathbf{BBR}^{4(+\bullet)}$ at concentrations of 0.050, 0.025, 0.0125, 0.00625, and 0.00313 mM. The absorption in the NIR region decreases linearly with the decreasing concentration (see inset), indicating intramolecular radical pairing.

5. Variable Temperature ^{1}H NMR Spectra

Variable temperature ^{1}H NMR spectra were recorded using an Agilent DD2 spectrometer with a 500 MHz working frequency for ^{1}H nuclei.

Variable Temperature ^{1}H NMR Spectra of BBR•8PF$_6$

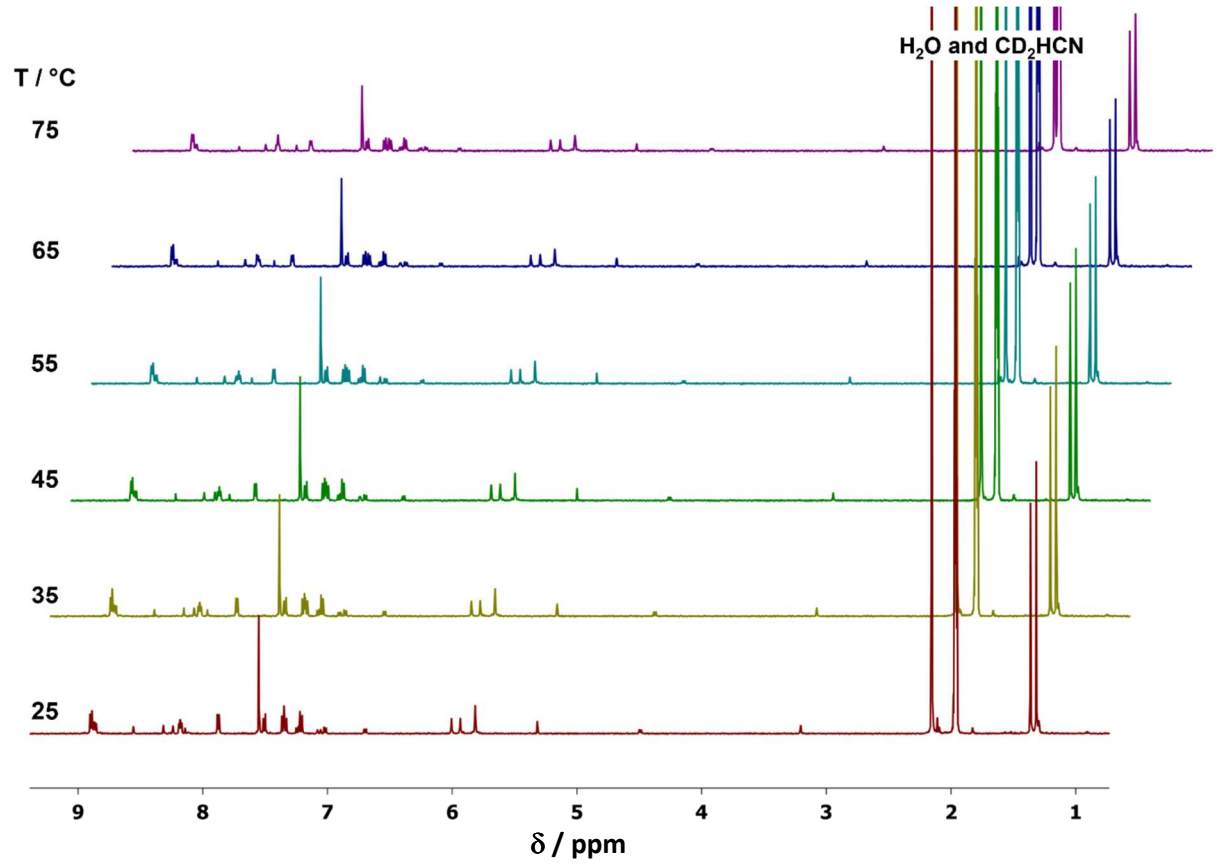

Figure S11. ^{1}H NMR spectra collected over a temperature range of 25 – 75 °C on a 1 mM solution of **BBR**•8PF$_6$ in CD_3CN. The full ^{1}H NMR spectrum is displayed for each temperature. Every resonance corresponding to **BBR**$^{8+}$ that is observed at 25 °C is also observed at 75 °C. All singlet resonances exhibit ≤ 2 Hz increase in peak width at half height over this temperature range, thus indicating that the rotaxane exhibits co-constitutional asymmetry on the ^{1}H NMR timescale over the temperature range of 25 – 75 °C.

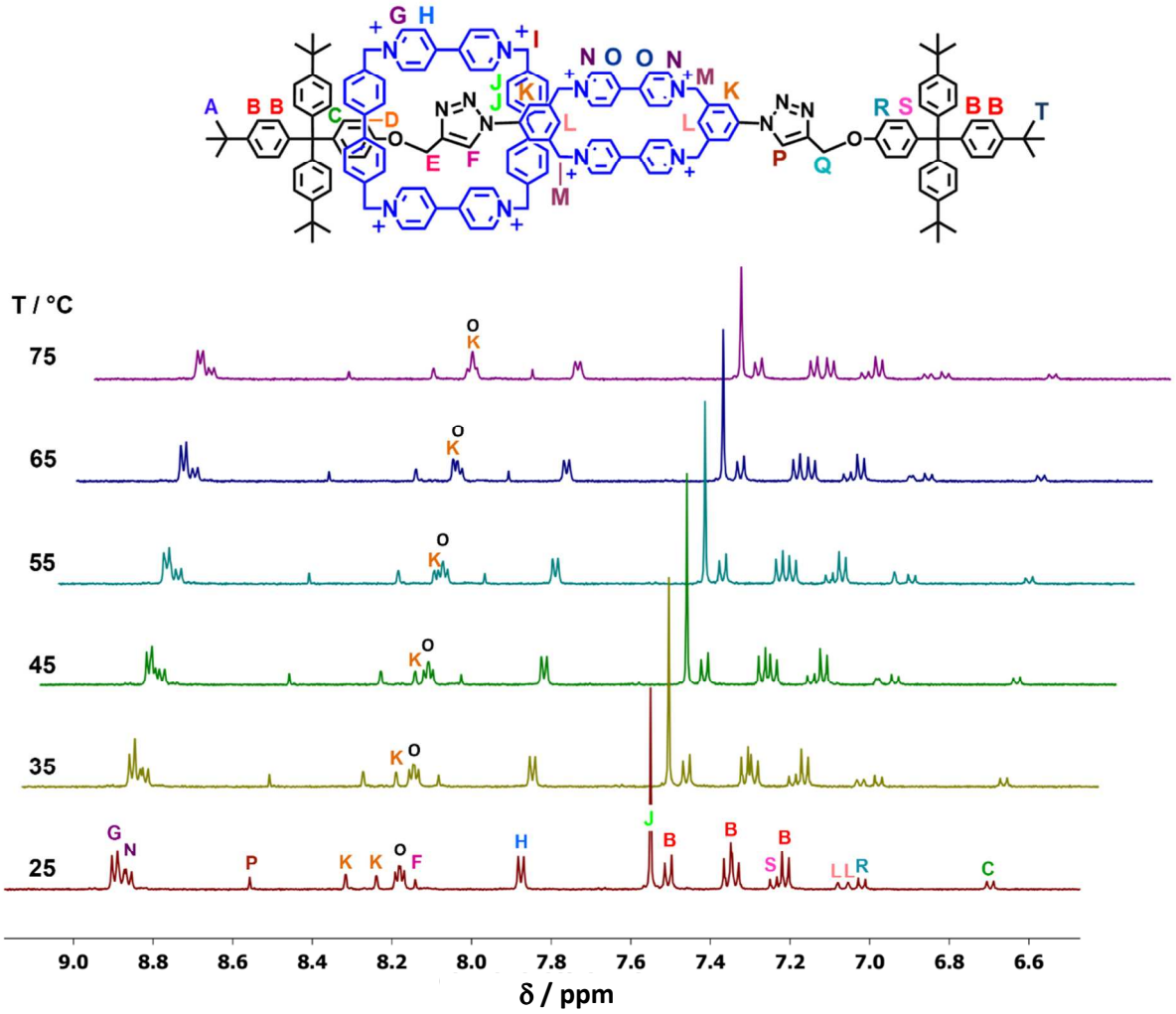

Figure S12. Partial ^{1}H NMR spectra of the aromatic region collected over a temperature range of 25 – 75 °C on a 1 mM solution of **BBR**•8PF_6 in CD_3CN. All resonances in this region are labeled in the 25 °C spectrum, while only select signals are labeled in the other spectra. The resonances labeled "O" correspond to C—H protons of the viologen units of the dumbbell, which are rendered anisochronous by the slow shuttling of the molecular square over the macrocyclic unit of the dumbbell. For the small separation (6.5 Hz at 75 °C) of these two resonances, a shuttling rate constant of 29 s^{-1} would result in coalescence.[5] Thus, the fact that two distinct O resonances remain sharply observable at 75 °C demonstrates that the shuttling rate of the square must be << 29 s^{-1} even at this elevated temperature. Note that one of the triazole C—H resonances, labeled K, overlaps with the two O resonances at 75 °C, but this situation does not prevent the observation of the O resonances as two distinct signals.

VT ^{1}H NMR Spectra of BBR$^{4(+\bullet)}$ (BBR•8PF$_6$ reduced over Zn)

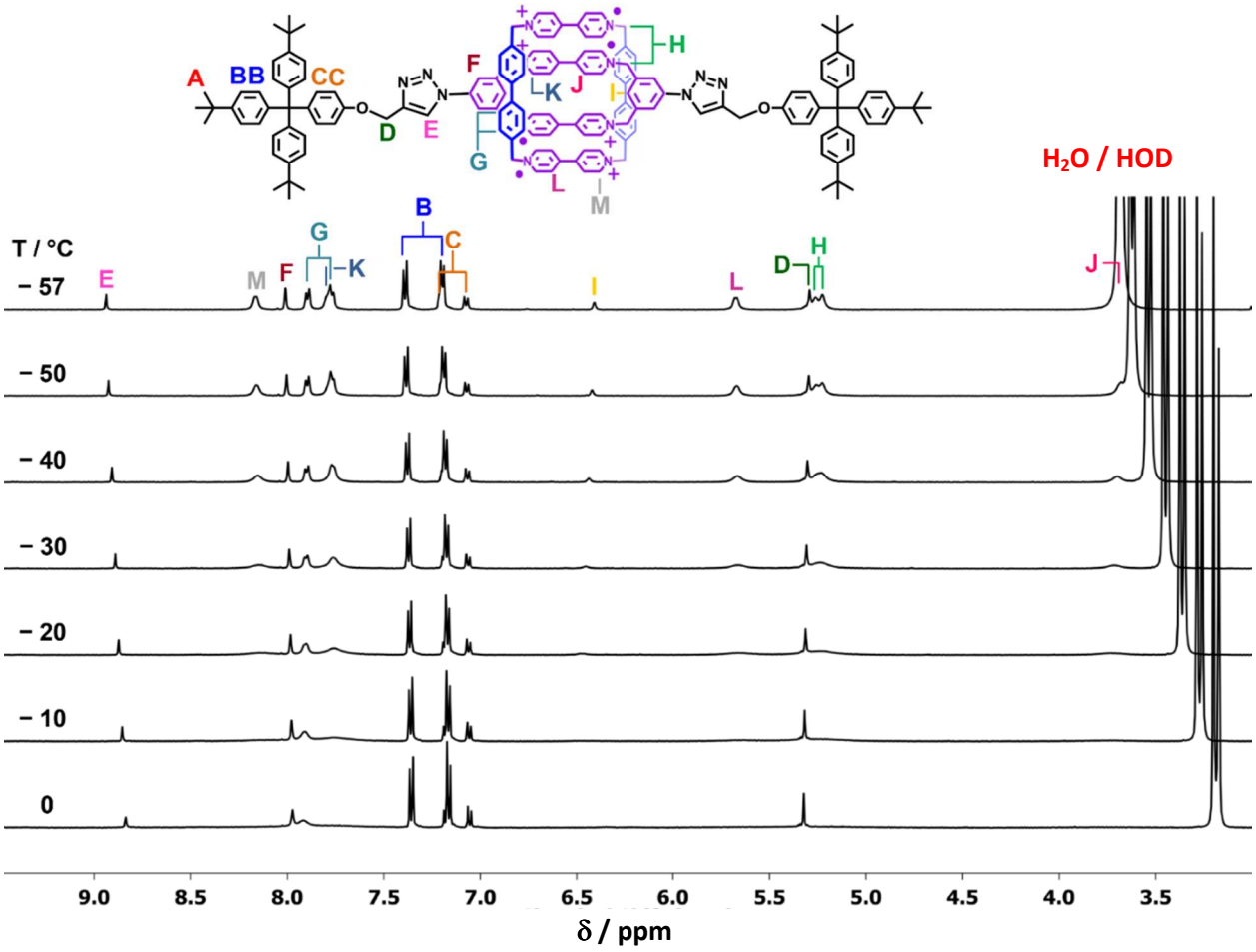

Figure S13. Partial ^{1}H NMR spectra displaying all but the alkyl region of a 1 mM solution of **BBR$^{4(+\bullet)}$** in CD_3COCD_3 over a temperature range of −57 to 0 °C. Note that −57 °C is lowest temperature that could be achieved using the automated chiller unit with which the spectrometer is equipped. All possible proton resonances are observable as relatively sharp signals at this temperature, with the exception of resonance "J", which is observed at −50 °C, but becomes obscured by the H_2O and HOD signals at −57 °C. See Figure S14 for a description of how the proton resonances of the viologen units were assigned.

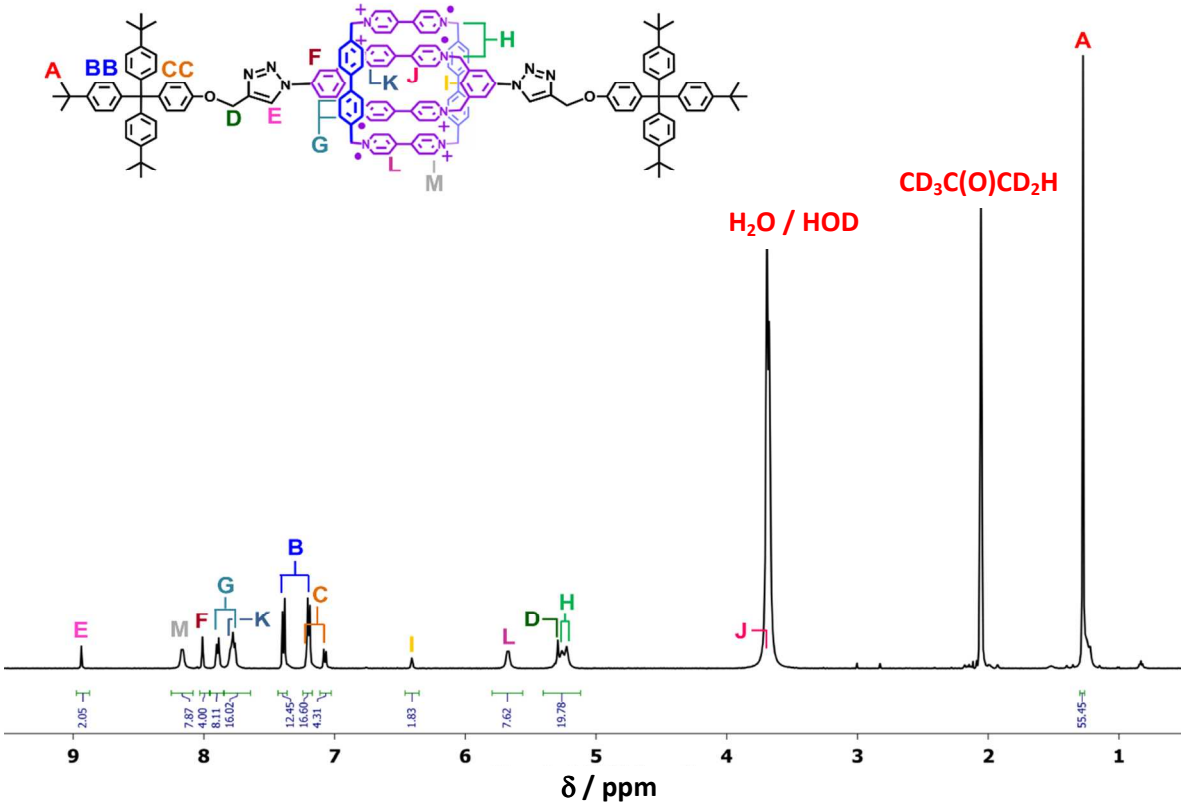

Figure S14. Full ^{1}H NMR spectrum of a 1 mM solution of **BBR**$^{4(+\bullet)}$ in CD_3COCD_3 that was collected at −57 °C. The assignments of most resonances were readily evident from the observed multiplicity, chemical shift, and integration of the signals. The four aromatic resonances of the viologen groups are, however, indistinguishable based on multiplicity and integration. Nevertheless, these resonances exhibit significantly different chemical shifts, such that assignments could be made based on the expected degree of shielding provided by the neighboring viologen units.

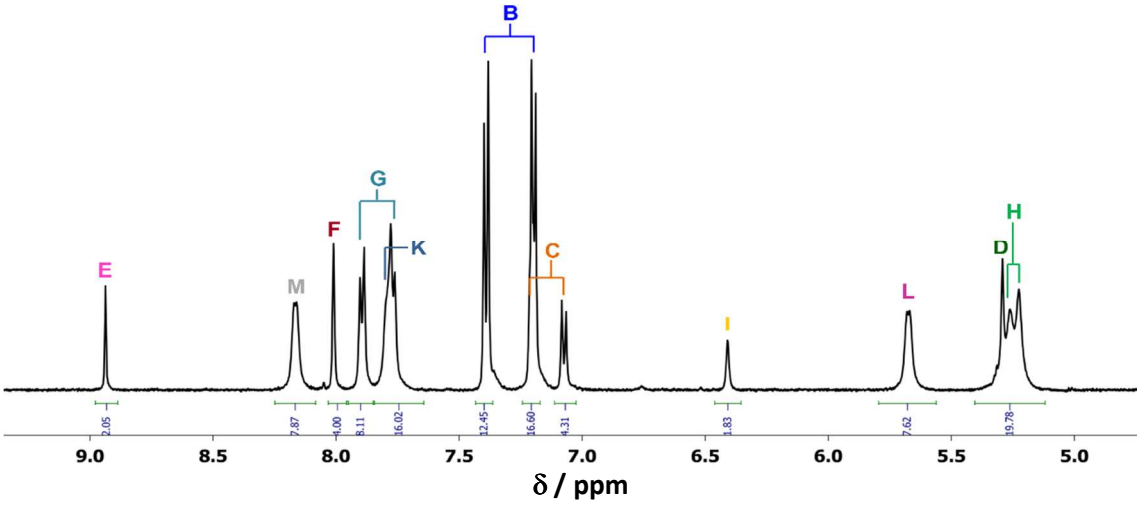

Figure S15. Partial ^{1}H NMR spectrum displaying the aromatic and methylene region of a 1 mM solution of **BBR**$^{4(+\bullet)}$ in CD_3COCD_3 that was collected at −57 °C.

6. Variable Temperature UV-Vis-NIR Spectra

Stock solutions of the octacationic **BBR**$^{8+}$ were prepared by dissolving suitable amounts of **BBR**•8PF_6 in air-free MeCN to provide a 0.5 mM concentration. A sample of **BBR**$^{4(+\bullet)}$ was prepared from this stock solution by stirring over activated Zn dust for 15 min to form a dark magenta-purple solution of the tetraradical tetracation **BBR**$^{4(+\bullet)}$. This solution was filtered and transferred to a 1 mm quartz cuvette that was fused to a short glass neck that terminates with a threaded PTFE stopper. This cuvette design ensures the rigorous exclusion of air for extended periods of heating and cooling the sample. A further reduced sample was prepared by treating the stock solution of **BBR**$^{8+}$ with 6 equiv of Cp_2Co. The concentration of the Cp_2Co stock solution was calibrated prior to use by the addition of a known volume to an excess of **MV**•2PF_6 solution, followed by measuring the resulting concentration of **MV**$^{(+\bullet)}$ by UV-Vis-NIR spectroscopy.

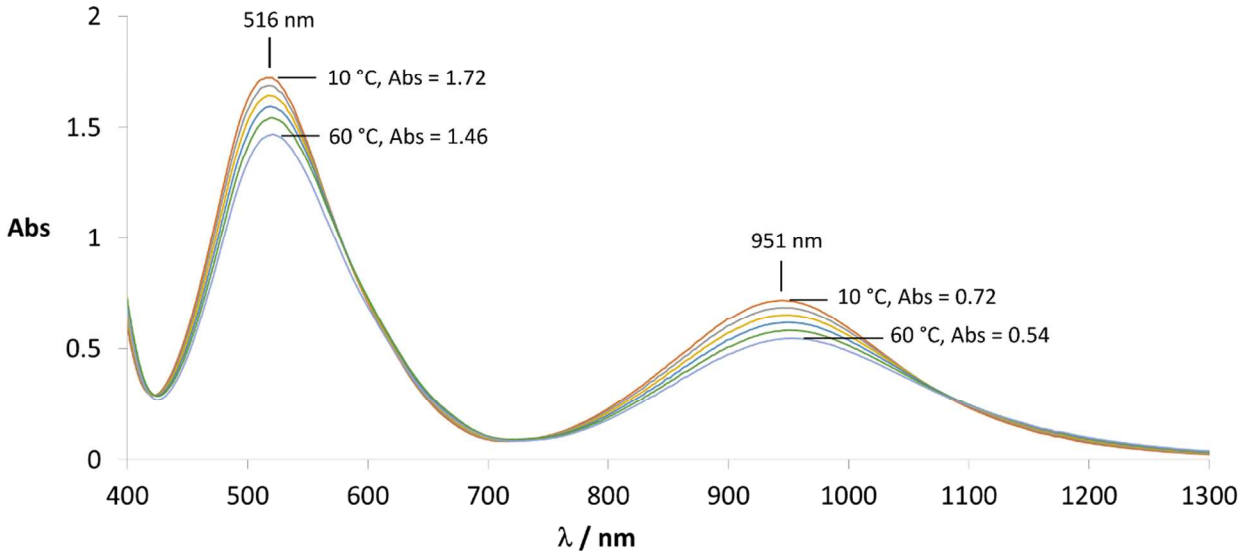

Figure S16. Variable temperature UV-Vis-NIR spectra of a 0.50 mM solution of **BBR**$^{4(+\bullet)}$ in MeCN measured over a range of 10 – 60 °C. Both the visible region absorption band (λ_{max} = 516 nm) and the NIR-band (λ_{max} = 951 nm) exhibit temperature-dependent changes in molar absorptivity. Note that previous studies of the supramolecular complex **[MS□*m*-CBPQT]**$^{4(+\bullet)}$ have shown that temperature dependent dissociation of the two diradical cyclophanes results in red-shifting of the visible region absorption without a significant decrease in the absorptivity.

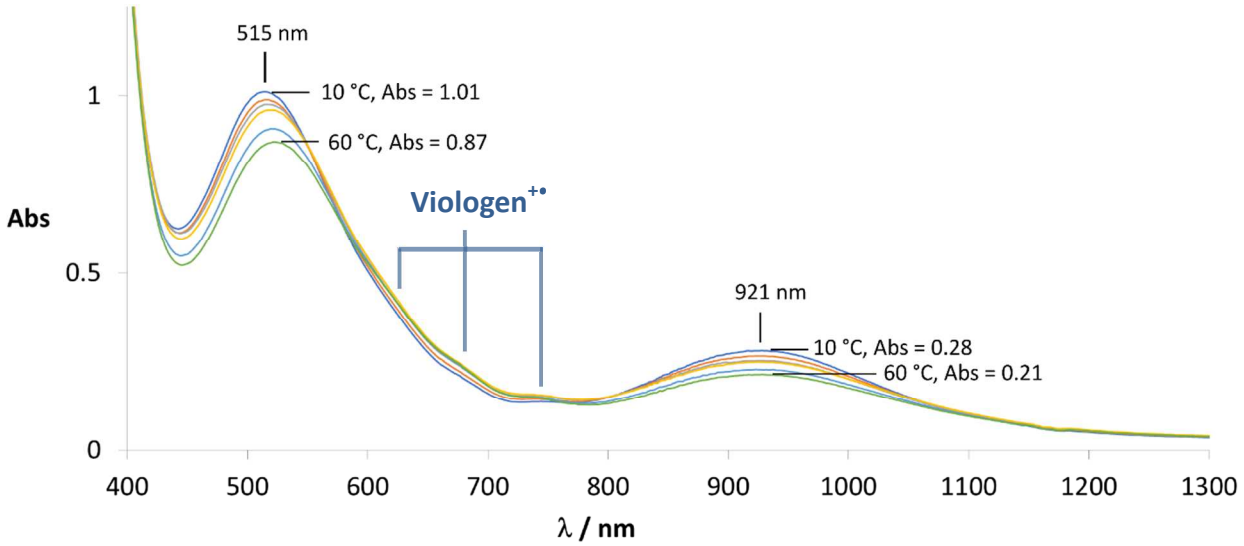

Figure S17. Variable temperature UV-Vis-NIR spectra (10 – 60 °C) of a 0.50 mM solution of **BBR**$^{8+}$ MeCN after being treated with 6 equiv of Cp_2Co. Both the visible region absorption band (λ_{max} = 515 nm) and the NIR-band (λ_{max} = 921 nm) exhibit temperature-dependent changes in molar absorptivity that are similar to those observed for the **BBR**$^{4(+\bullet)}$ state of the rotaxane. For the sample reduced using 6 equiv of Cp_2Co, however, there were features in the visible region of the spectrum that increased slightly at higher temperatures. These features are consistent with the presence of unpaired viologen radical cationic units.

7.i. UV-Vis-NIR Monitoring of Titration of BBR^{8+} with Cp_2Co

A solution of **BBR**•8PF_6 (0.050 mM in MeCN) was titrated with 1 equiv at a time of Cp_2Co. All measurements were collected at 298 K in a 1 cm path length cell equipped with a screw-cap. The concentration of the stock solution of Cp_2Co in MeCN was calibrated by adding 10 μL to a 1.00 mL solution containing a large excess of **MV**•2PF_6 in MeCN. The resulting concentration of **MV**$^{+\bullet}$ was determined by comparing the UV-Vis spectrum of the solution to UV-Vis data reported[6] in the literature for **MV**$^{+\bullet}$, and the concentration of the radical cation was used to determine the concentration of the Cp_2Co stock solution. A microliter syringe was then employed to add 1 equiv of coboltocene at a time to the solution of **BBR**$^{8+}$ in MeCN. A spectrum of the sample was collected before adding any cobaltocene, and then after each addition up to a total of ≥ 8 equiv of Cp_2Co. Similar procedures were used for titrations conducted at other concentrations and using other solvents, e.g., Me_2CO and Me_2SO.

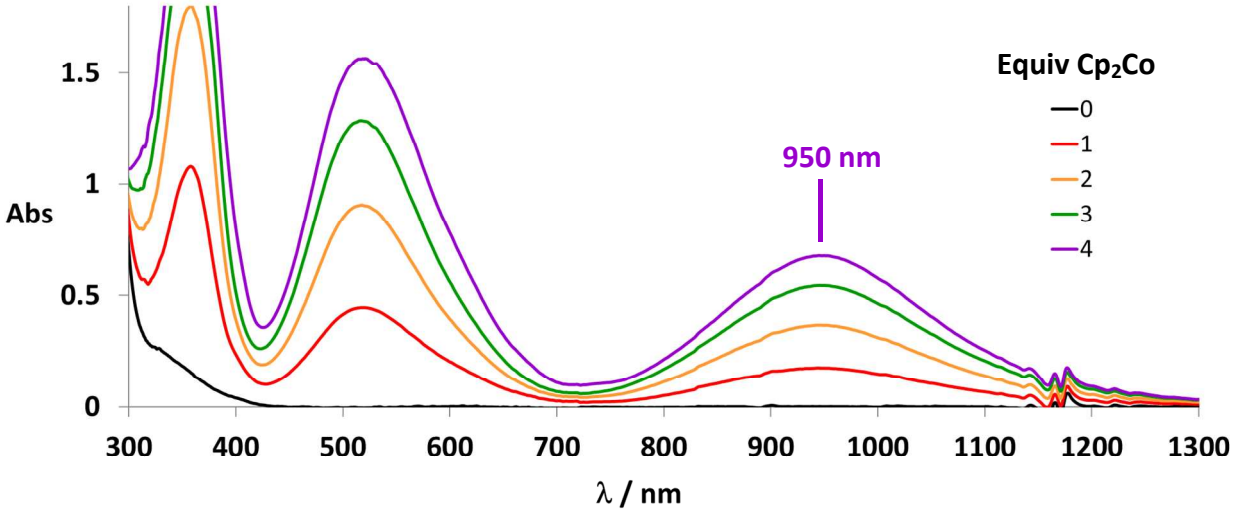

Figure S18. UV-Vis-NIR monitoring of the addition of 0 – 4 equiv of Cp_2Co to an MeCN solution of **BBR**•$8PF_6$ (0.050 mM) in a 1 cm cuvette. The absorption bands in the visible and NIR regions increase approximately linearly with each equivalent of Cp_2Co that was added.

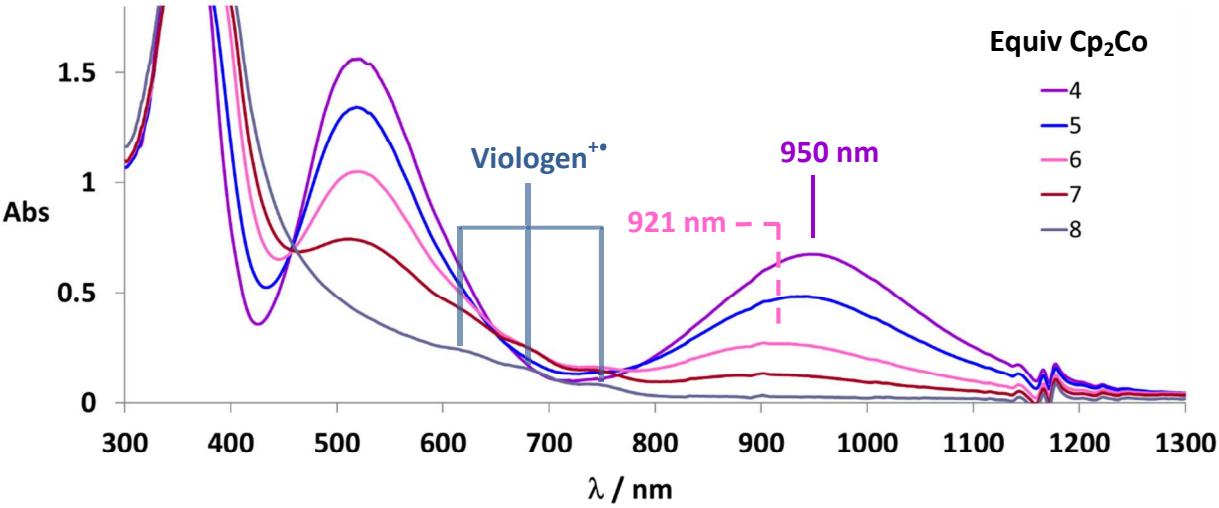

Figure S19. UV-Vis-NIR monitoring of the addition of 4 – 8 equiv of Cp_2Co to an MeCN solution of **BBR**•$8PF_6$ (0.050 mM) in a 1 cm cuvette. The absorption in the NIR region decreases in two large steps upon the addition of the 5th and 6th equiv of Cp_2Co. These decreases are accompanied by a blue shifting of the NIR absorption from λ_{max} = 950 nm to λ_{max} = 921 nm. Addition of two more equiv of Cp_2Co resulted in the NIR absorption decreasing over two smaller steps, until almost completely disappearing after adding the 8th equiv of Cp_2Co. At this point, features were evident in the visible region of the spectrum that indicate the presence of unpaired viologen radicals, suggesting that a small amount of the rotaxane was not fully reduced.

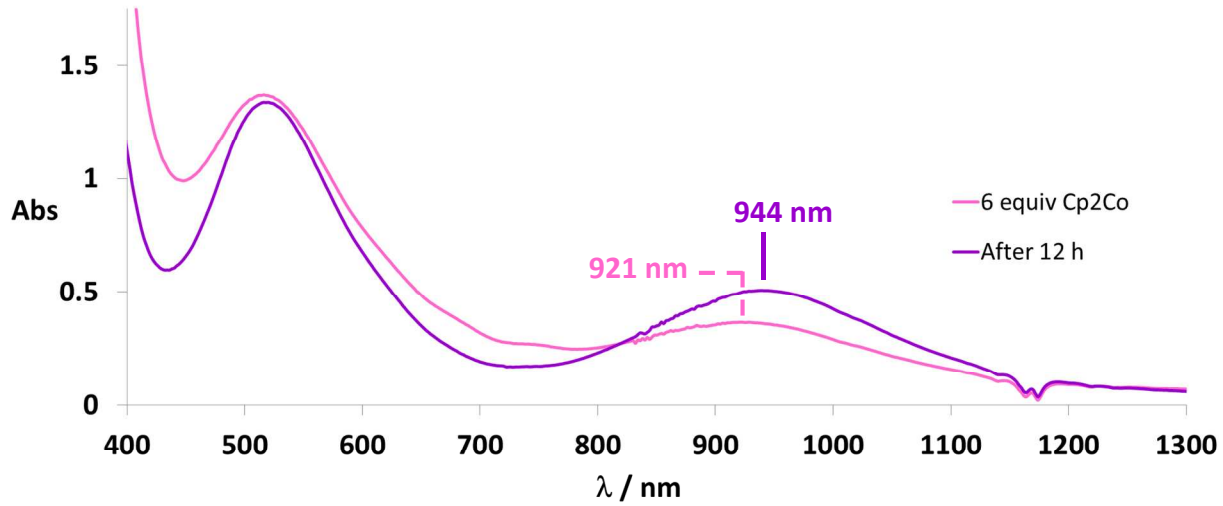

Figure S20. UV-Vis-NIR spectrum of a solution of **BBR**•8PF_6 (0.4 mM) in MeCN in a 2 mm cuvette after the addition of 6 equiv of Cp_2Co. The sample was stored inside an N_2 glovebox for 12 h, after which a precipitate had formed and the NIR absorption increased in intensity and exhibited a red-shift from λ_{max} = 920 nm to λ_{max} = 944 nm. These observations are attributed to the disproportionation of $\mathbf{BBR}^{2(+\bullet)}$ to form $\mathbf{BBR}^{4(+\bullet)}$ and the insoluble $\mathbf{BBR}^{0}$.

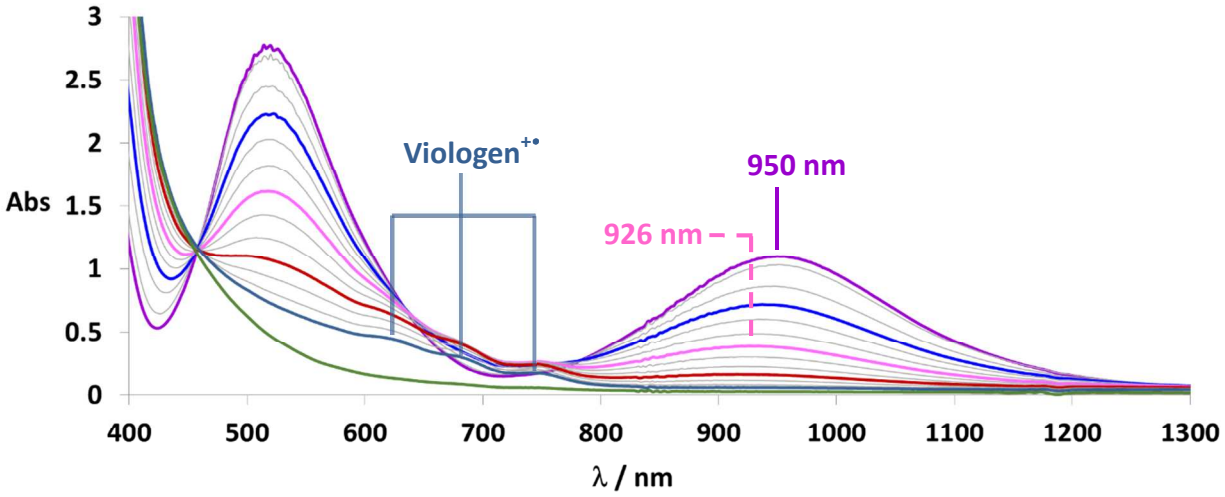

Figure S21. UV-Vis-NIR monitoring of the addition of 4 – 8 equiv of Cp_2Co in 1/3 equiv portions to an Me_2CO solution of **BBR**•8PF_6 (0.33 mM) in a 2 mm cuvette. The NIR absorption band decreases significantly between adding 4 and 6 equiv of Cp_2Co, and these decreases are accompanied by a blue shift of this band from λ_{max} = 950 nm to λ_{max} = 926 nm. Further addition of Cp_2Co resulted in the NIR absorption decreasing over smaller steps, until almost completely disappearing after the addition of 8 equiv of Cp_2Co. At this point, due to incomplete electron transfer, features were evident in the visible region of the spectrum that indicated the presence of unpaired viologen radicals. These features disappeared upon the addition of an excess of Cp_2Co (14 equiv), indicating full reduction of the rotaxane to the neutral $\mathbf{BBR}^{0}$ state.

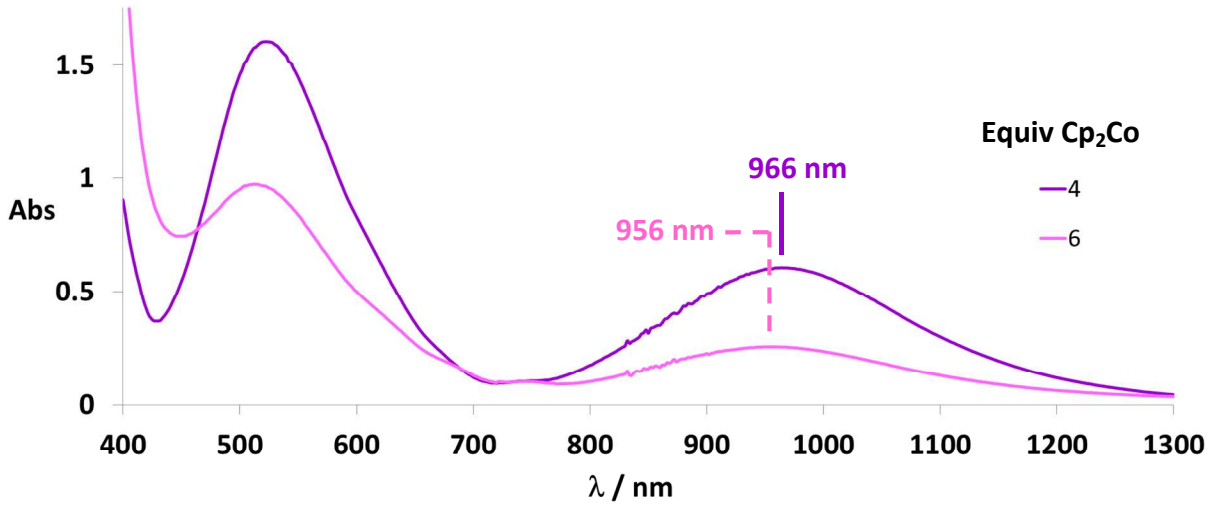

Figure S22. UV-Vis-NIR spectra after the addition of 4 and 6 equiv of Cp_2Co to an Me_2SO solution of **BBR**•$8PF_6$ (0.25 mM) in a 2 mm cuvette. In contrast to Cp_2Co titrations of the rotaxane in MeCN and Me_2CO, the NIR absorption exhibited only slight blue-shifting between adding the 4th and 6th equiv of Cp_2Co, suggesting that **BBR**$^{4(+\bullet)}$ is the only major radically paired species that is accessible in Me_2SO, even after the addition of > 4 equiv of reductant.

7.ii. ^{1}H NMR Monitoring of Titration of BBR^{8+} with Cp_2Co

A solution of **BBR**•$8PF_6$ (0.60 mM in CD_3CN) was titrated with 1 equiv at a time of a Cp_2Co solution in CD_3CN, and ^{1}H NMR spectra were collected after each addition using a Bruker Avance III spectrometer with a 500 MHz working frequency for ^{1}H nuclei. The concentration of the stock solution of Cp_2Co in CD_3CN was calibrated by adding 5 μL to a 1.00 mL solution containing an excess of **MV**•$2PF_6$ in MeCN. The resulting concentration of **MV**$^{+\bullet}$ was determined by comparing the UV-Vis spectrum of the solution to UV-Vis data reported[6] in the literature for **MV**$^{+\bullet}$. A glass microliter syringe was used to measure and dispense the coboltocene solution into the solution of **BBR**•$8PF_6$. A sealed capillary tube containing ferrocene in CD_3CN was added as an internal standard.

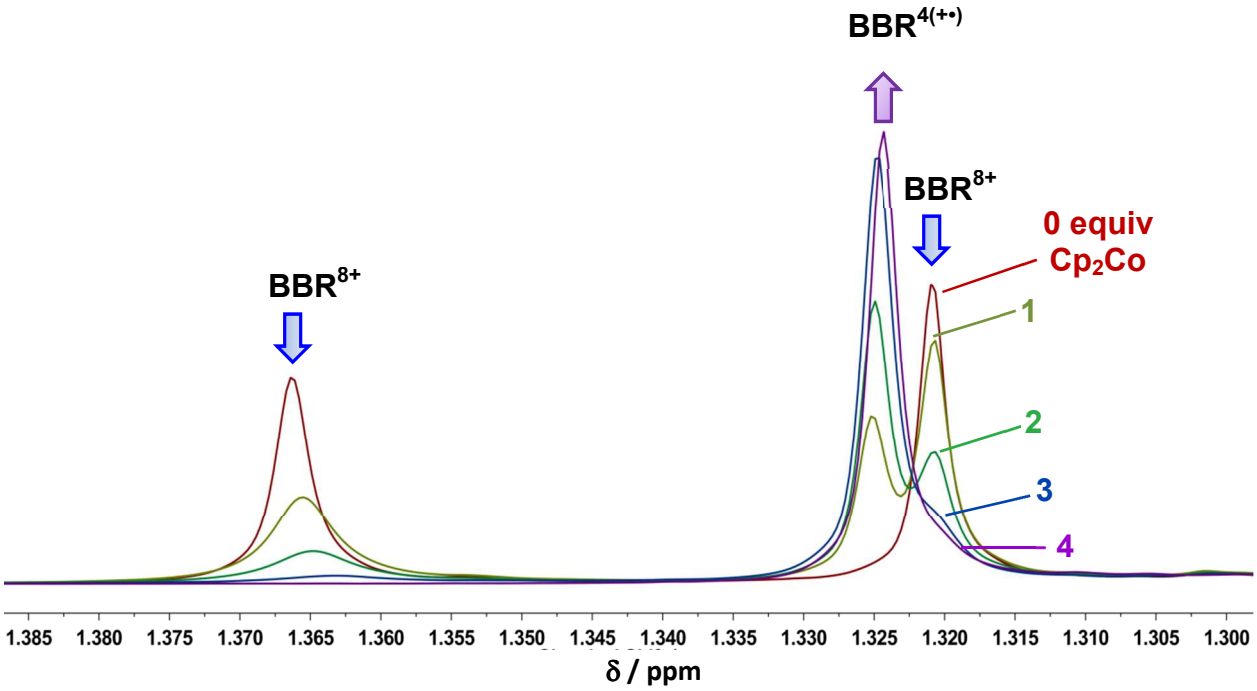

Figure S23. The partial ^{1}H NMR spectra, displaying the alkyl region, of a solution of **BBR**•8PF_6 after the addition of 0 – 4 equiv of Cp_2Co. The ^{t}Bu resonances of **BBR**$^{8+}$ decrease as Cp_2Co is added, while the single ^{t}Bu resonance of the co-constitutionally symmetric rotaxane **BBR**$^{4(+•)}$ increases. Note that the more downfield resonance of **BBR**$^{8+}$ exhibits significant broadening upon adding the first equiv of Cp_2Co, while this behavior is not observed for the more upfield resonance as **BBR**$^{8+}$ is converted to **BBR**$^{4(+•)}$.

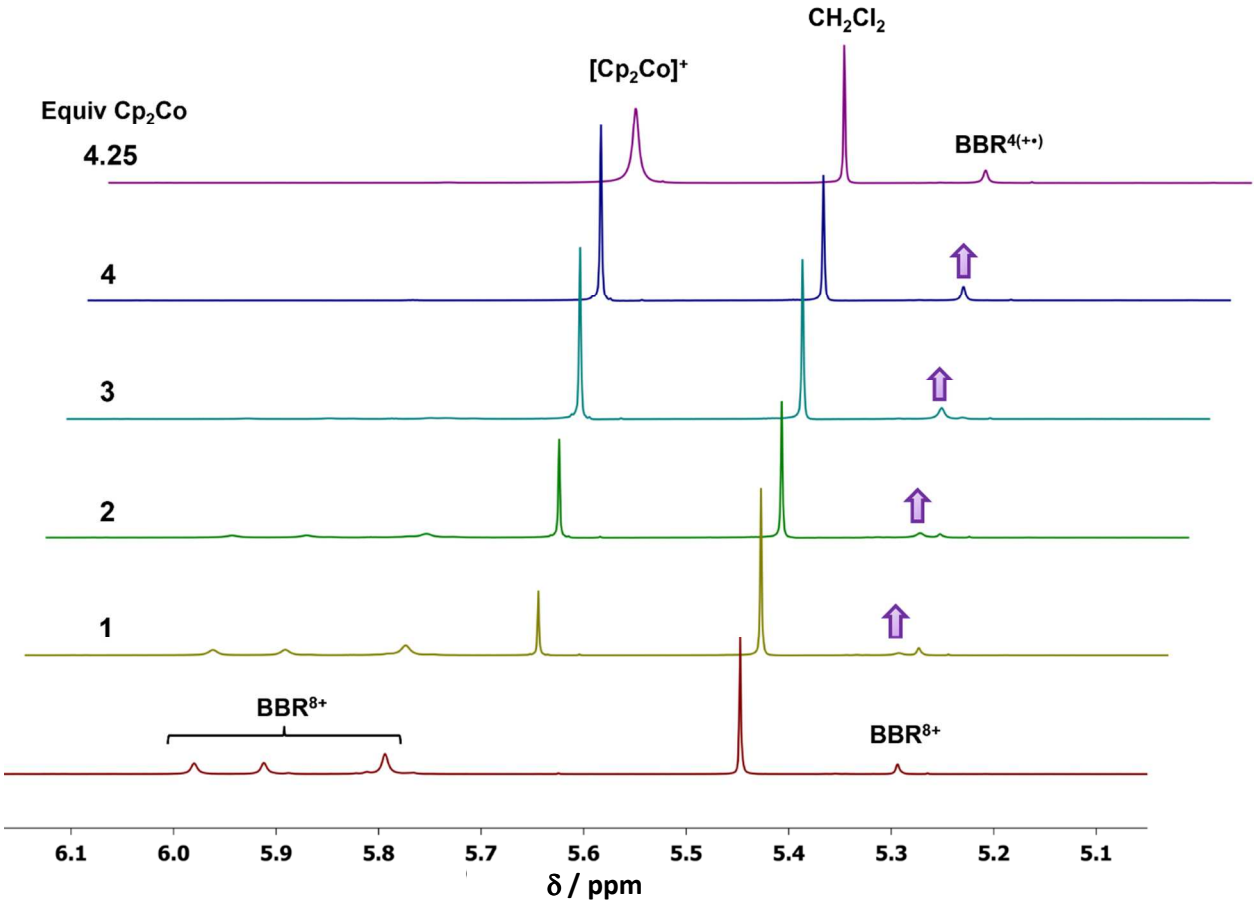

Figure S24. The partial ^{1}H NMR spectra in the methylene region (NCH_2− and $ArOCH_2$−) of a solution of **BBR**•$8PF_6$ after addition of 0 – 4.25 equiv of Cp_2Co. The resonances of $\mathbf{BBR}^{8+}$ decrease in intensity as Cp_2Co is added and a new $ArOCH_2$− resonance, marked with arrows, appears for $\mathbf{BBR}^{4(+\bullet)}$. The reductant, Cp_2Co, is converted to the diamagnetic cation $[Cp_2Co]^+$. Note that the ^{1}H NMR resonance of $[Cp_2Co]^+$ is broadened and shifted slightly upfield after adding >4 equiv of Cp_2Co, which is attributed to rapid degenerate electron exchange with the small excess of paramagnetic Cp_2Co present in solution. See Figure S29 for a view of this portion of the spectra obtained after the addition of > 4.25 equiv of Cp_2Co, in which very broad resonances corresponding to Cp_2Co^+/Cp_2Co.

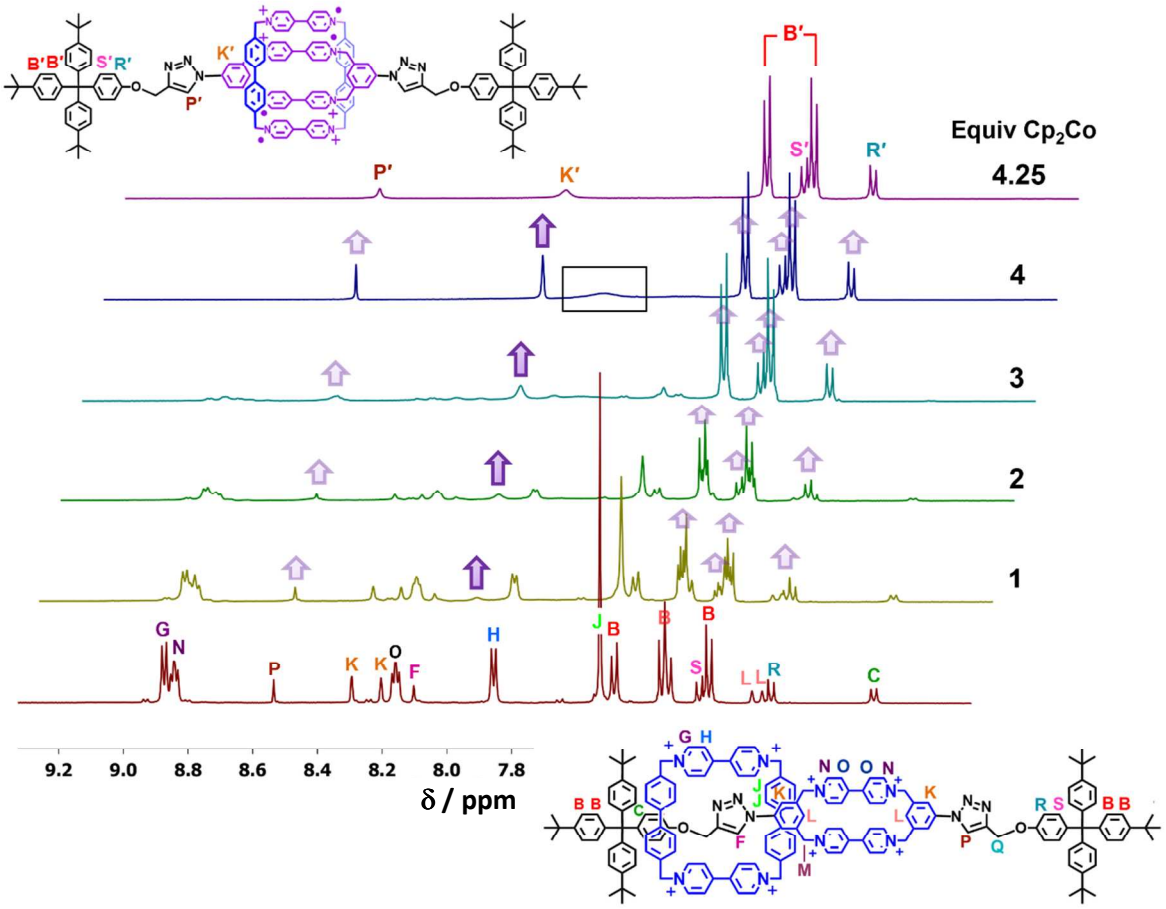

Figure S25. The partial ^{1}H NMR spectra in the aromatic region of a solution of **BBR**•8PF_6 after addition of 0 – 4.25 equiv of Cp_2Co. The resonances of $\mathbf{BBR}^{8+}$ decrease as Cp_2Co is added, until completely disappearing after addition of 4 equiv. Arrows are used to mark the increase of resonances corresponding to $\mathbf{BBR}^{4(+\bullet)}$. Smaller faded arrows are used to indicate resonances that appear in positions that overlap with those of $\mathbf{BBR}^{8+}$. Resonances P′ and K′ (top) of $\mathbf{BBR}^{4(+\bullet)}$ are sharpest in the spectrum collected after the addition of 4 equiv of Cp_2Co. Since these signals are the nearest easily observable resonances to the viologen units in $\mathbf{BBR}^{4(+\bullet)}$, the broadening may be caused by the slight accessibility of paramagnetic states of the viologens, such as a 3+ or 5+ trisradical state of the rotaxane depending on whether more than or less than 4 equiv of Cp_2Co has been added. Similarly, a very broad resonance, highlighted above inside a rectangle, is observed after adding 4 equiv of Cp_2Co, but disappears after the addition of >4 equiv. This broad resonance can be assigned definitively to the biphenylene linker of the square cyclophane based upon variable temperature ^{1}H NMR studies of $\mathbf{BBR}^{4(+\bullet)}$. See Figure S13 for VT NMR.

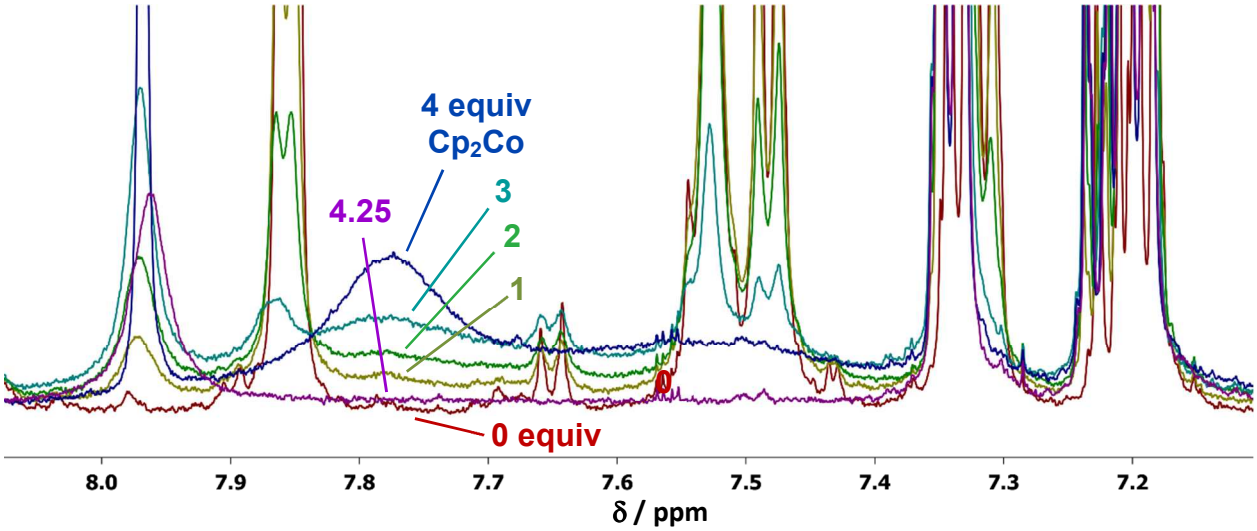

Figure S26. Partial ^{1}H NMR spectra displaying a portion of the aromatic region of a solution of **BBR**•8PF$_6$ after the addition of 0 – 4.25 equiv of Cp_2Co. The ^{1}H NMR resonances of the biphenylene linker are observed as a very broad signal that increases from 1 – 4 equiv of Cp_2Co, but then disappears after addition of >4 equiv of Cp_2Co. The disappearance of this resonance after the addition of >4 equiv of Cp_2Co can be attributed to an increase in the radical character of the cyclophane units of the rotaxane in lower oxidation states. See EPR data in Section 8 for direct observation of the increase in radical character.

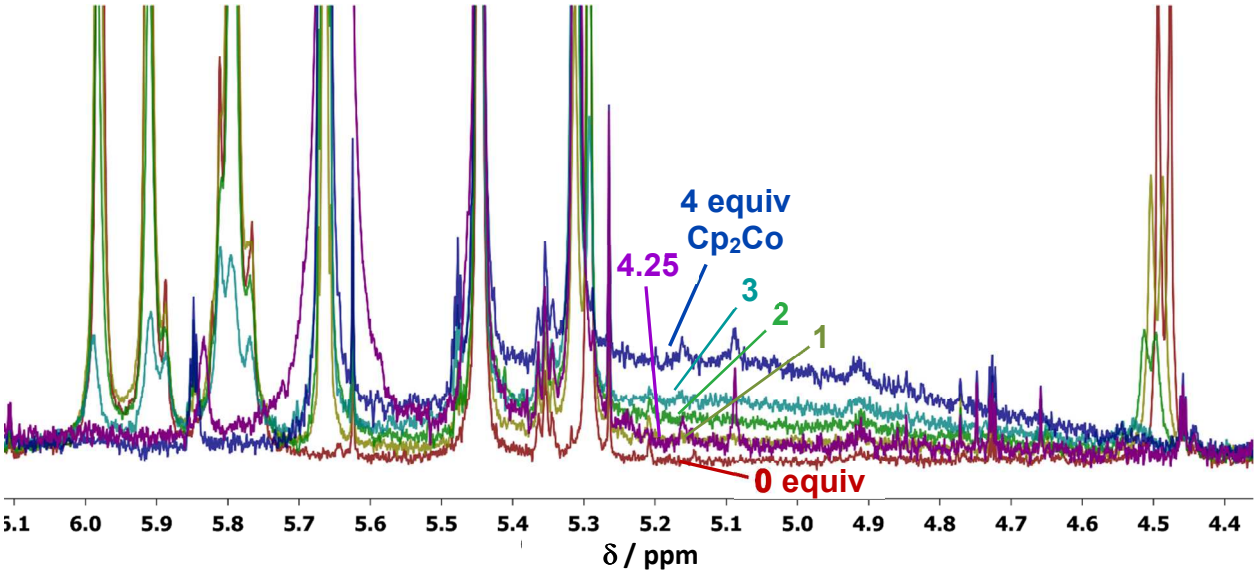

Figure S27. Partial ^{1}H NMR spectra of the methylene region of **BBR**•8PF$_6$ after the addition of 0 – 4.25 equiv of Cp_2Co. The *N*-methylene groups are observed as broad resonances that increase as Cp_2Co is added, up to 4 equiv of the reductant, then disappear upon addition of >4 equiv.

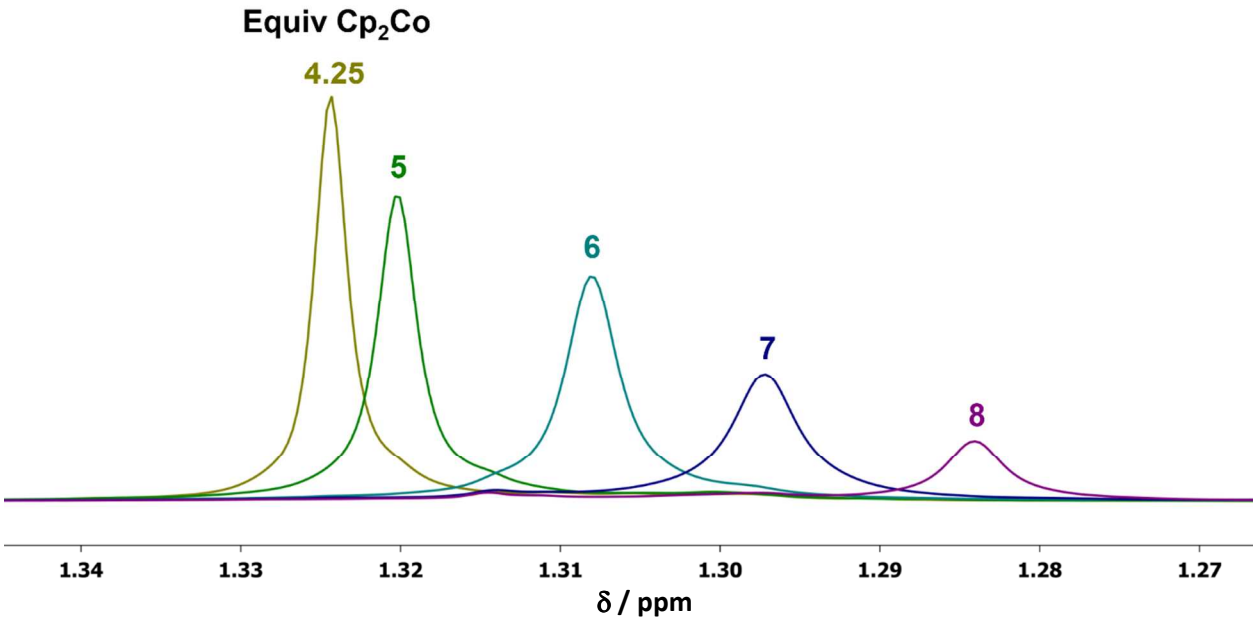

Figure S28. Partial ^{1}H NMR spectra in the alkyl region of a solution of **BBR**•8PF_6 after addition of 4.25 – 8 equiv of Cp_2Co. Only a single ^{t}Bu resonance is observed after all additions of Cp_2Co beyond 4 equiv, even when half integer equivalents are added, i.e., 4.5, 6, 6.5, 7 etc. (not shown), thus demonstrating that this ^{t}Bu resonance must arise from the rapid interconversion of multiple oxidation states of the rotaxane.

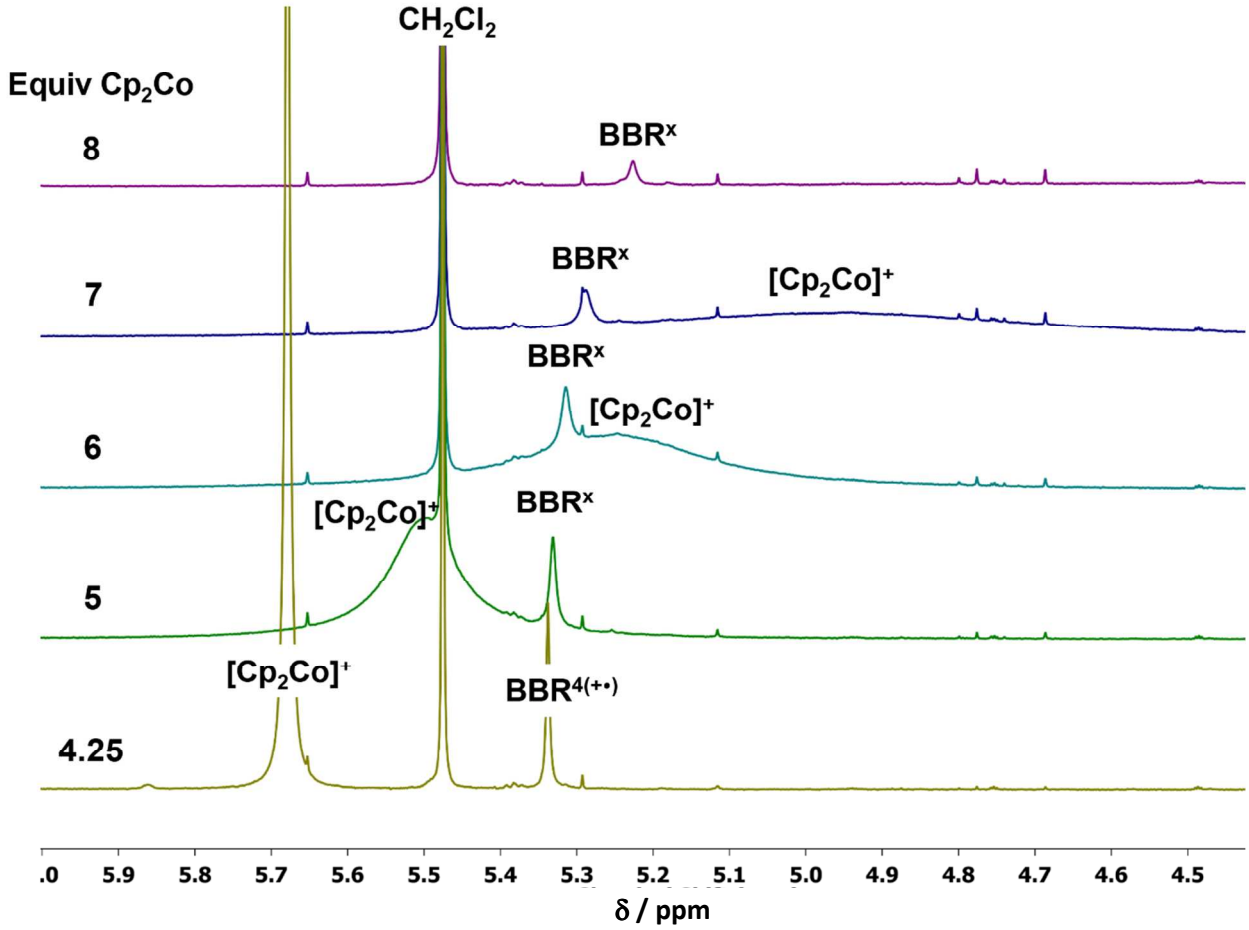

Figure S29. Partial ^{1}H NMR spectra in the methylene region of a solution of **BBR**•8PF_6 after the addition of 4.25 – 8 equiv of Cp_2Co. The only resonance observed in this region for $\mathbf{BBR}^{\mathbf{4(+\bullet)}}$ is the $ArOCH_2-$ resonance, which is labeled $\mathbf{BBR}^{\mathbf{4(+\bullet)}}$ in the spectrum collected after adding 4.25 equiv of Cp_2Co since the rotaxane is, at this point, primarily residing in this state. The label $\mathbf{BBR}^{\mathbf{x}}$ is used in the remaining spectra to indicate that, in these spectra, this resonance arises from multiple interconverting oxidation states of the rotaxane. The reductant, Cp_2Co, is converted to the diamagnetic cation $[Cp_2Co]^+$, but the ^{1}H NMR resonance of $[Cp_2Co]^+$ is significantly broadened and shifted upfield after successive additions of Cp_2Co. This behavior is attributed to rapid degenerate electron exchange between $[Cp_2Co]^+$ and a small, but increasing, concentration of paramagnetic Cp_2Co that is present in solution as a result of incomplete electron transfer to the rotaxane.

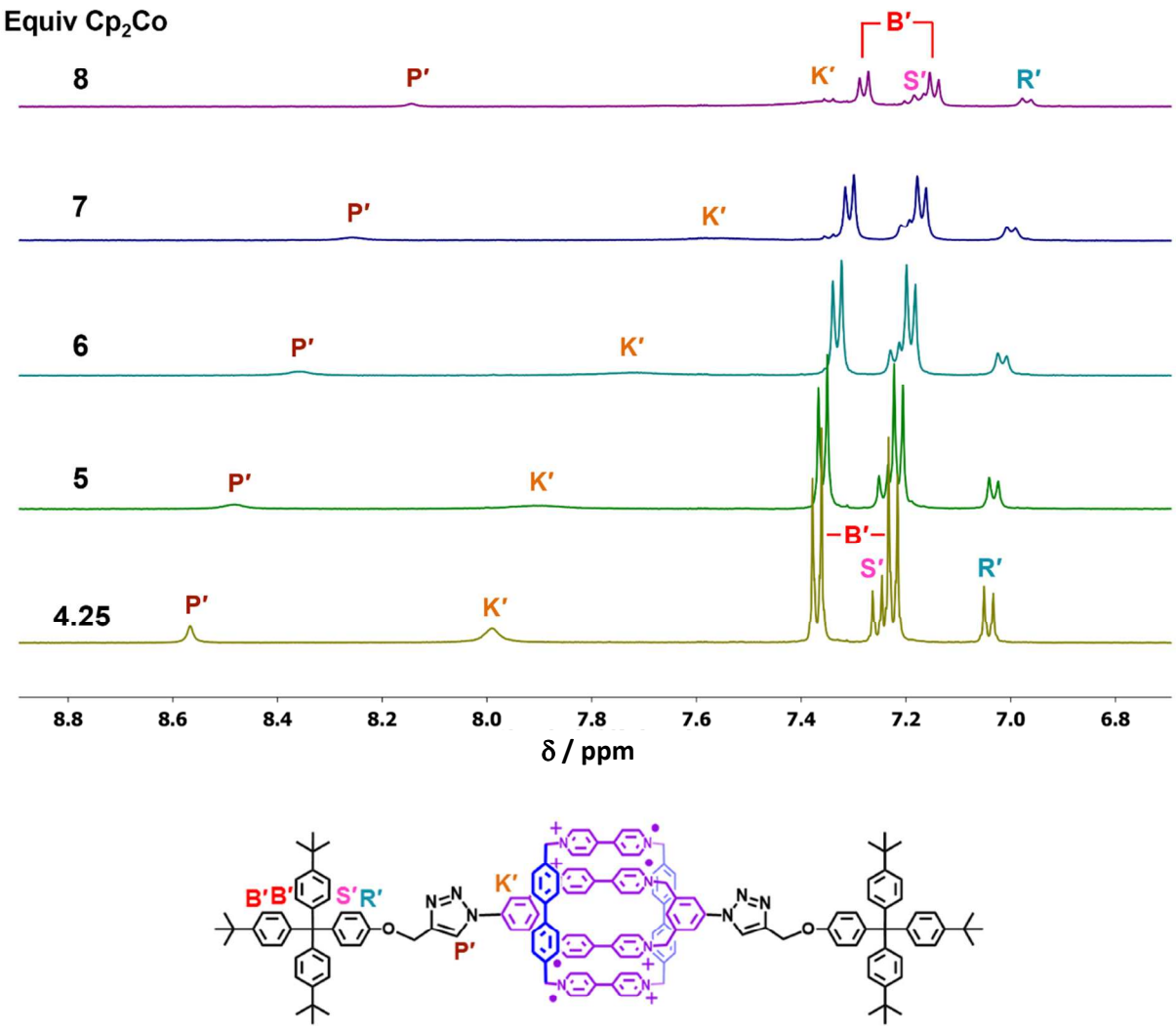

Figure S30. Partial ^{1}H NMR spectra in the aromatic region of a solution of **BBR**•8PF_6 after the addition of 4.25 – 8 equiv of Cp_2Co. Resonances **B′**, **R′**, and **S′**, which correspond to the stopper group, remain sharp in all of these spectra, while resonances **P′** and **K′**, which are nearer to the radical cation viologen units, exhibit significant broadening as additional equivalents of Cp_2Co are added.

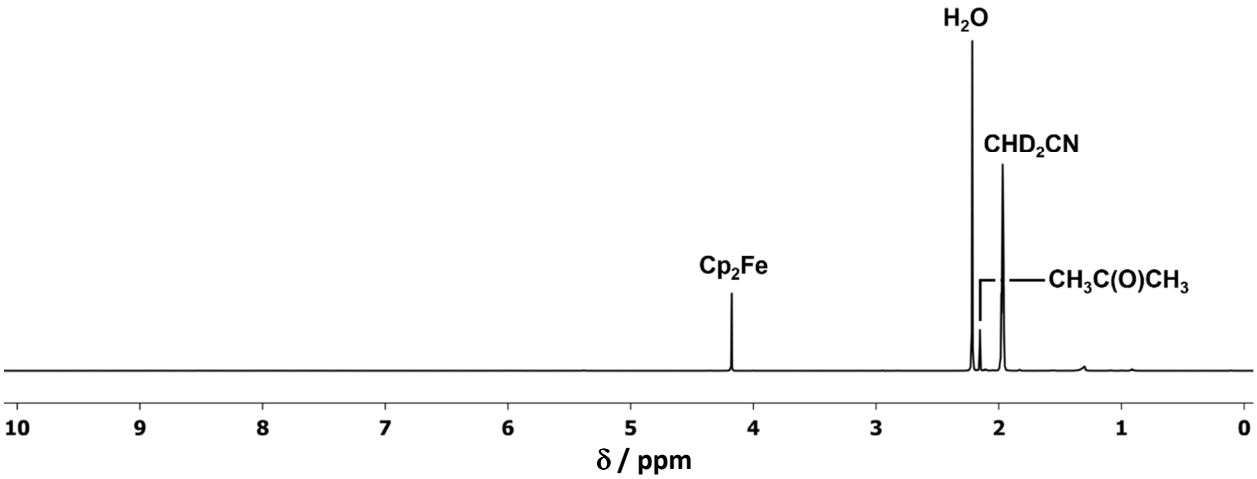

Figure S31. ^{1}H NMR spectrum of a 1:1 ratio mixture of ***o*-CBPQT$^{2(+\bullet)}$** and ***o*-CBPQT^{4+}** (0.5 mM each) that was prepared by mixing a colorless 1 mM solution of ***o*-CBPQT•**$4PF_6$ with an equal volume of a dark magenta solution of ***o*-CBPQT$^{2(+\bullet)}$** to provide a dark blue solution. The only observed resonances correspond to CHD_2CN, H_2O, a ferrocene internal standard, and trace solvent impurities.

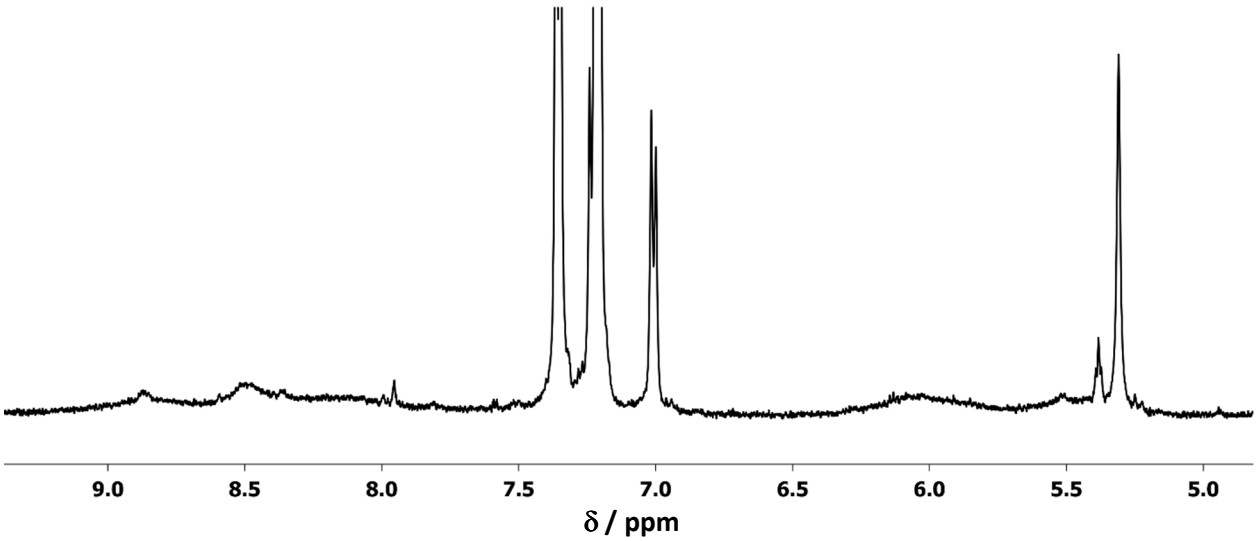

Figure S32. ^{1}H NMR spectrum of a 1:1 ratio mixture of ***m*-BDB$^{2(+\bullet)}$** and ***m*-BDB^{4+}** (0.5 mM each) that was prepared by mixing a 1 mM solution of ***m*-BDB** •$4PF_6$ with an equal volume of a 1 mM solution of ***m*-BDB$^{2(+\bullet)}$**. Resonances corresponding to the stopper groups of the dumbbell are observed as sharp signals, while the only other observable resonances are very broad and poorly defined.

7.iii. EPR Spectroscopic Monitoring of Titration of BBR^{8+} with Cp_2Co

Procedure 1: Microliter syringes were used to measure the appropriate amounts of a solution of **BBR**•$8PF_6$ (1.00 mM in MeCN) and a solution of Cp_2Co in MeCN (calibrated as described above for UV-Vis-NIR and ^1H NMR titrations) to prepare samples containing 0 – 8 equiv of Cp_2Co relative to the rotaxane. The resulting solutions were then diluted with MeCN to provide 0.50 mM concentrations of the rotaxane. A 100 μL amount of each sample was transferred to a quartz EPR tube and sealed with UV-cured epoxy resin. EPR Spectra were then collected at the X-band (2.8712 GHz) at 298 K.

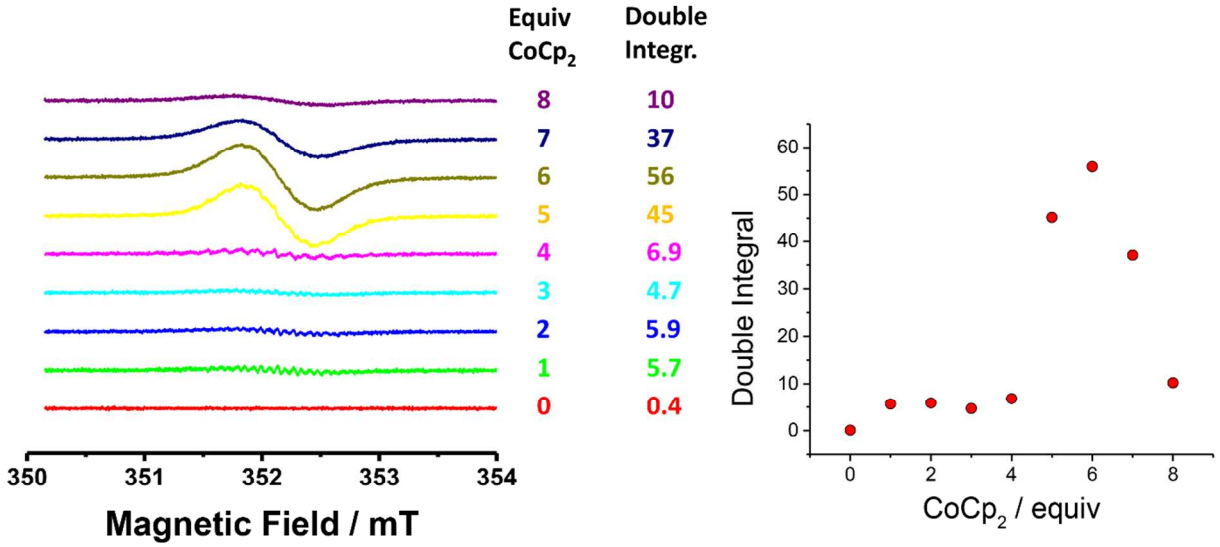

Figure S33. EPR Spectra (left) collected after reducing 0.50 mM solutions of **BBR**•$8PF_6$ in MeCN with 0 – 8 equiv of Cp_2Co. The integrated signal intensity of each spectrum is plotted on the right. Precipitate was observed in the samples containing 7 and 8 equiv of the reductant, which appears to be at least partially responsible for the decrease in EPR signal intensity in these samples. See Figure S34 for similar experiments employing acetone as the solvent, which was found to better solvate the lower oxidation states of the rotaxane.

Procedure 2: A microliter syringe was used to titrate a solution of Cp_2Co in MeCN into a quartz cuvette containing a 0.33 mM solution of **BBR**•$8PF_6$ in Me_2CO. Initially, 4 equiv of Cp_2Co was added, followed by 1/3 equiv additions until a total of 8 equiv was reached, followed by an additional 6 equiv (14 total). UV-Vis-NIR spectra were recorded after each addition (see Figure S21), and aliquots were removed after 4, 5, 6, 7, 8, and 14 equiv. The aliquots were diluted with additional Me_2CO to provide 0.25 mM concentrations of the rotaxane. The resulting solutions were transferred to quartz EPR tubes and flame sealed prior to collecting EPR spectra at 298 K.

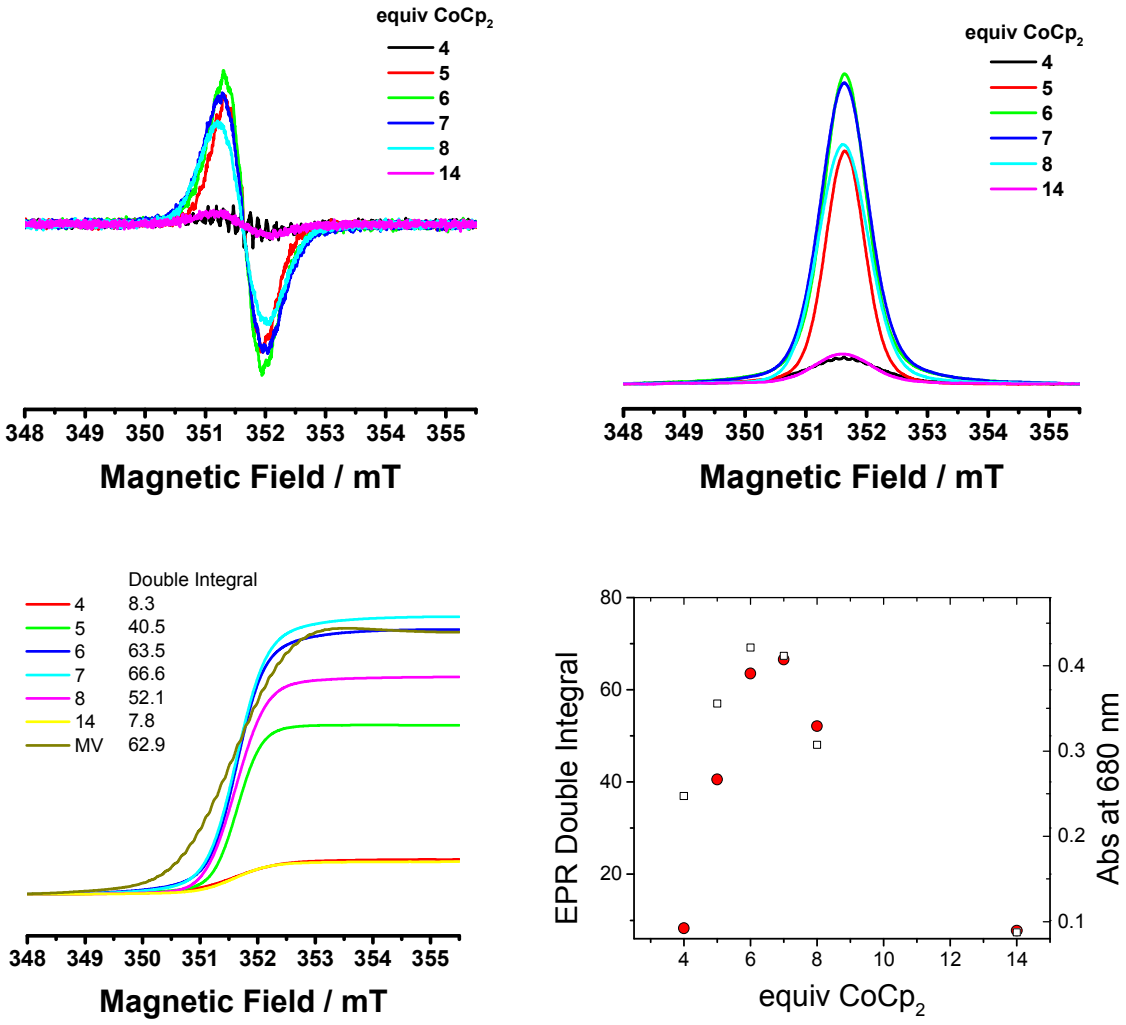

Figure S34. EPR spectra (top left and right) of 0.25 mM solutions of **BBR**•$8PF_6$ in $CH_3C(O)CH_3$ after adding 4, 5, 6, 7, 8, and 14 equiv of Cp_2Co. The integrated signal intensity of each spectrum is presented in the bottom left and right images. The integrated signal intensity of a 0.22 mM solution of $\mathbf{MV}^{+\bullet}$ is included in the bottom left image. In the bottom right image, the integrated signal intensities of the rotaxane EPR signals (red circles) are compared with the UV-Vis absorbance (white squares) associated with unpaired viologen radicals in each sample.

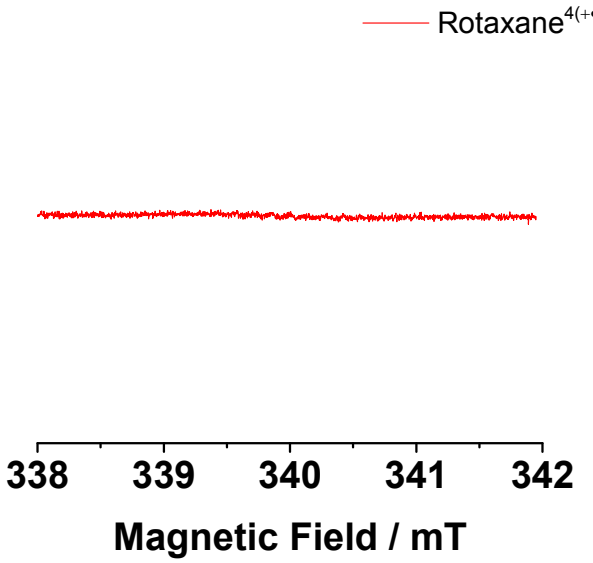

Figure S35. EPR Spectrum collected after reducing a 0.50 mM solutions of **BBR**•8PF_6 in MeCN over Zn dust. Only a very faint signal can be discerned in this spectrum, indicating that this method of reduction results in nearly quantitative formation of the diamagnetic **BBR**$^{4(+•)}$ state of this rotaxane. The very slight signal that is observed in this spectrum is attributed to the presence of a very small quantity of the free dumbbell component ***m*-BDB2**$^{(+•)}$ in the sample.

8. Cyclic Voltammetry

Samples for cyclic voltammetry were prepared using an electrolyte solution of 0.1 M [Bu_4N][PF_6] in MeCN that was sparged with Ar to remove O_2. Cyclic voltammograms were recorded under Ar or N_2 using a glassy carbon working electrode, a Pt counter electrode, and an Ag wire pseudo-reference electrode. Reported potentials are referenced to the Fc/Fc^+ redox couple of a ferrocene internal standard. The rotaxane exhibits two redox couples, but at concentrations of $\geq$ 0.25 mM, the more negative redox couple exhibits an unusual type of quasi-reversibility (see Figure S35), which is attributed to interaction of the analyte with the electrode surface. This redox couple exhibited normal reversible behavior at 0.125 mM concentrations of **BBR**•8PF_6, and thus, subsequent CVs were recorded at this concentration. The lower analyte concentration also diminished fouling of the electrode surface over multiple scans.

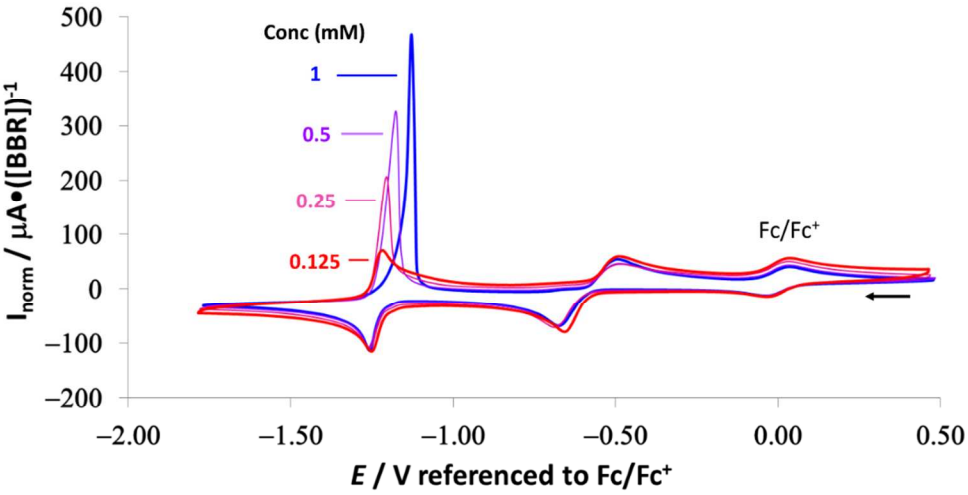

Figure S36. Cyclic voltammograms of **BBR**•8PF_6 measured at a scan rate of 0.2 V/s with concentrations of 0.125, 0.25, 0.50, and 1.0 mM of the rotaxane. An arrow marks the direction in which the potential was scanned. The current is scaled proportionally to the rotaxane concentration, which provides consistent values for the more positive redox couple as well as the more negative reduction wave, while the more negative re-oxidation wave exhibits an unexpectedly large peak current at concentrations ≥ 0.25 mM.

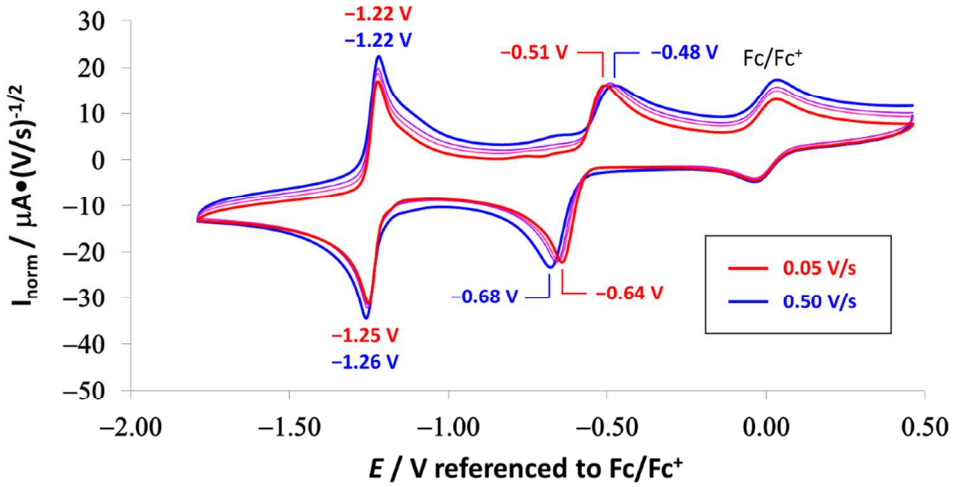

Figure S37. Cyclic voltammograms of a 0.125 mM solution of **BBR**•8PF_6 measured at scan rates of 0.050 – 0.50 V/s. The current of each reduction and oxidation wave scales proportionally to the square root of the scan rate, which is consistent with electrochemically reversible redox processes. The more positive redox couple, however, exhibits large separation between E_{pc} and E_{pa} (ΔE_p = 130 mV at 0.050 V/s) even at low scan rates, which indicates that these reduction and oxidation events do not correspond to a truly reversible redox couple. The observed irreversibility is attributed to 1) the stabilization of the radical state of each viologen unit by pairing of each radical electron, and 2) slow kinetics for the association/dissociation of the diradical square cyclophane and the diradical cyclophane recognition unit of the dumbbell.

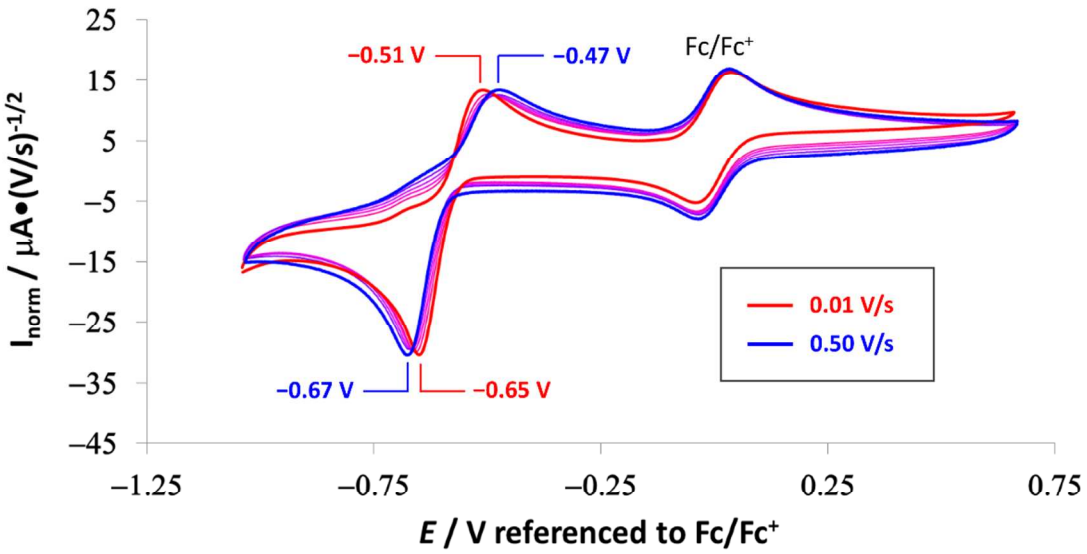

Figure S38. Cyclic voltammograms of a 0.125 mM solution of **BBR**•8PF_6 measured at scan rates of 0.010 – 0.50 V/s over a potential window that includes only the more positive redox couple of the rotaxane. Under these conditions, this redox couple exhibits similar behavior to that which is observed (Figure S26) when using a larger potential window.

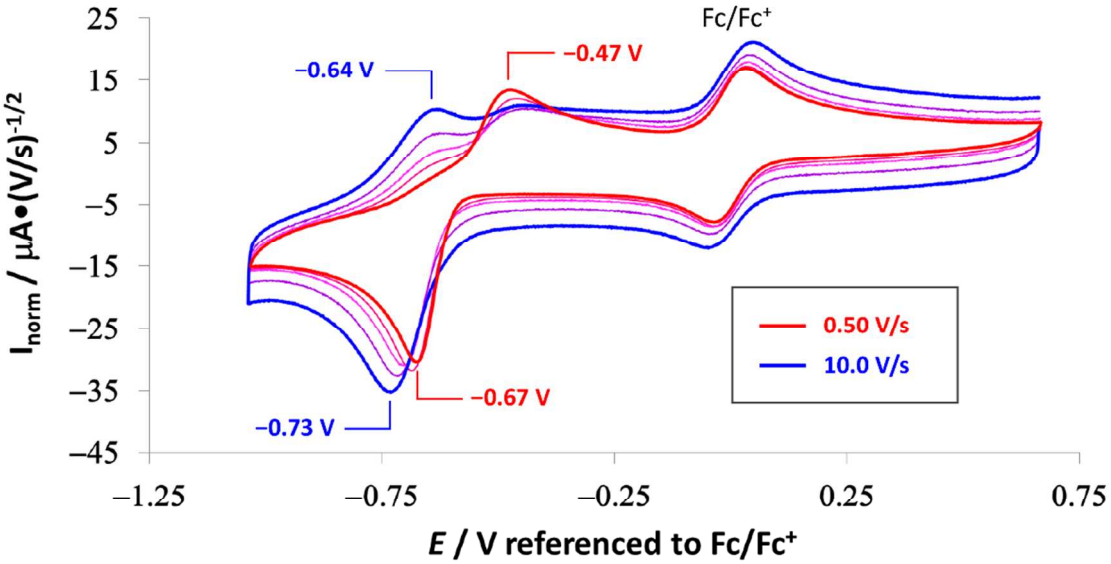

Figure S39. Cyclic voltammograms of a 0.125 mM solution of **BBR**•8PF_6 measured at scan rates of 0.50 – 10.0 V/s over a potential window that includes only the more positive redox couple of the rotaxane. As the scan rate is increased beyond 0.50 V/s, a new re-oxidation wave appears at potentials that are negative relative to those observed for re-oxidation at slower scan rates. This new oxidation wave is attributed to the oxidation of a metastable co-conformation of $\mathbf{BBR}^{4(+\bullet)}$ that does not exhibit radical-pairing interactions.

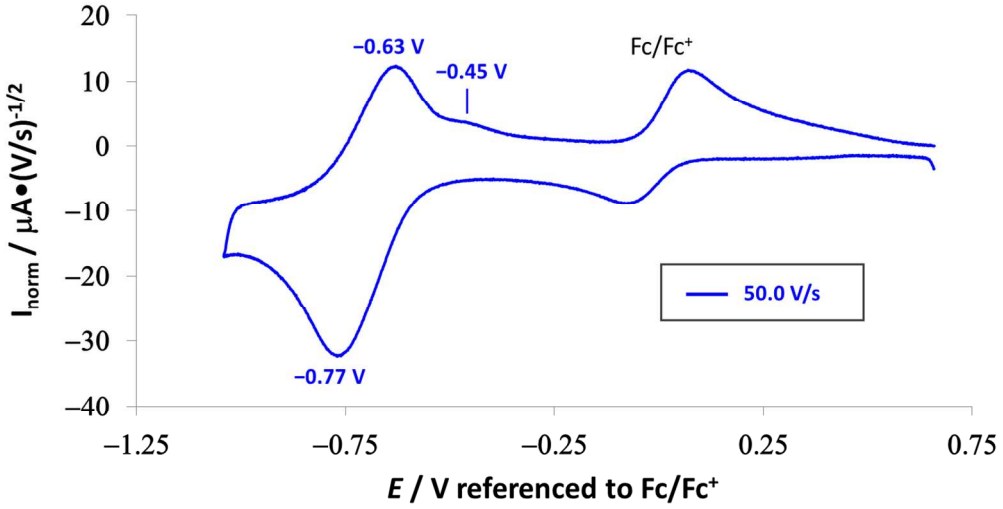

Figure S40. Cyclic voltammogram of a 0.125 mM solution of **BBR**•$8PF_6$ measured at a scan rate of 50.0 V/s over a potential window that includes only the more positive redox couple of the rotaxane. The re-oxidation wave (-0.45 V) corresponding to the radical-paired co-conformation has almost completely disappeared, while the redox couple involving the open-shell metastable co-conformation appears as nearly completely reversible. Note that the capacitive current, which was measured using 0.1 M $TBAPF_6$ in MeCN at 50V/s in the absence of redox active analytes, was subtracted from this CV.

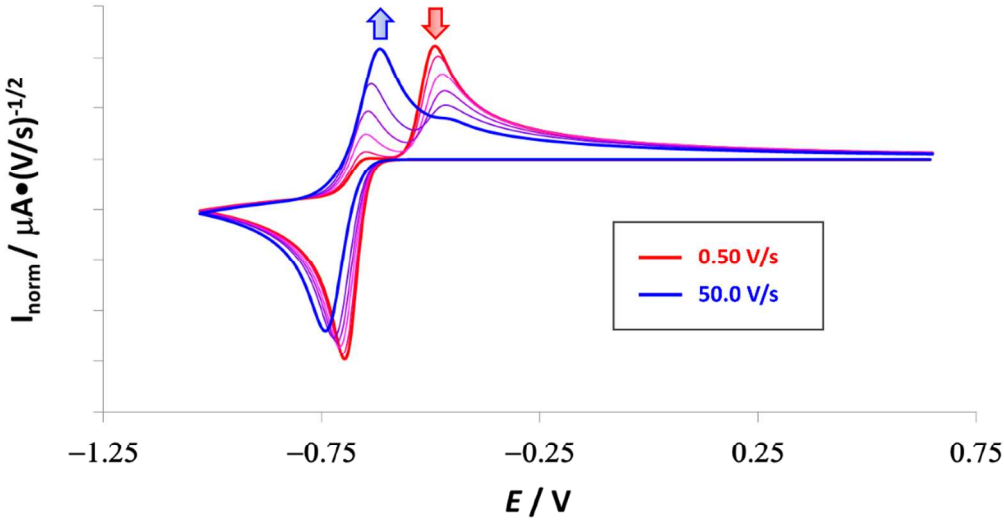

Figure S41. Simulated cyclic voltammograms of the more positive redox couple of $\mathbf{BBR}^{8+}$ at scan rates of 0.5, 1, 2.5, 5, 10, and 50 V/s using the electrochemical mechanism depicted in Scheme 4 of the main text. The rate constant, k_2, for conversion of the metastable open-shell co-conformation $\mathbf{BBR}^{4(+\bullet)}_{\mathbf{D}}$ to the closed-shell co-conformation $\mathbf{BBR}^{4(+\bullet)}_{\mathbf{A}}$ was optimized (k_2 = 15 s^{-1}) for best agreement with the experimental CVs. The arrows mark the disappearance and growth of the oxidation waves with increasing scan rates.

9. References

1. Asakawa, M.; Ashton, P. R.; Menzer, S.; Raymo, F. M.; Stoddart, J. F.; White, A. J. P.; Williams, D. J. Cyclobis(Paraquat-4,4′-Biphenylene)–an Organic Molecular Square. *Chem. Eur. J.* **1996**, *2*, 877 – 893.

2. Aucagne, V.; Hänni, K. D.; Leigh, D. A.; Lusby, P. J.; Walker, D. B. Catalytic "Click" Rotaxanes: A Substoichiometric Metal-Template Pathway to Mechanically Interlocked Architectures. *J. Am. Chem. Soc.* **2006**, *128*, 2186 – 2187.

3. Neelarapu, R.; Holzle, D. L.; Velaparthi, S.; Bai, H.; Brunsteiner, M.; Blond, S. Y.; Petukhov, P. A. Design, Synthesis, Docking, and Biological Evaluation of Novel Diazide-Containing Isoxazole- and Pyrazole-Based Histone Deacetylase Probes. *J. Med. Chem.* **2011**, *54*, 4350 – 4364.

4. Lipke, M. C.; Cheng, T.; Wu, Y.; Arslan, H.; Xiao, H.; Wasielewski, M. R.; Goddard, W. A. III; Stoddart, J. F. Size-Matched Radical Multivalency *J. Am. Chem. Soc.* **2017**, *139*, 3986 – 3998.

5. Bryant, R. G. The NMR time scale. *J. Chem. Educ.* **1983**, *60*, 933- 935.

6. Thorneley, R. N. F. A convenient electrochemical preparation of reduced methyl viologen and a kinetic study of the reaction with oxygen using an anaerobic stopped-flow apparatus. *Biochim. Biophys. Acta* **1974**, *333*, 487 – 496.